Commercial Aircraft Trajectory Optimization in a Vertical Plane: General Solutions Using Singular Control Theory

Amin Jafarimoghaddam[a*] ***Manuel Soler***[a]

ajafarim@pa.uc3m.es **masolera@ing.uc3m.es**

[a]*Department of Bioengineering and Aerospace Engineering, Universidad Carlos III de Madrid. Avenida de la Universidad, 30, Leganes, 28911 Madrid, Spain*

Abstract

A mathematical framework is developed to solve the commercial aircraft trajectory optimization problem in a vertical plane for a general case. The generality refers to an arbitrary objective function, a spatial wind field, a dual-element control vector, and a set of constraints. The original problem is singular on one of the control elements and regular on the other. Due to the small aerodynamic path angle, which is typical of commercial aircraft flights, and a large time scale separation between the flight dynamics, it is conventional to take the aerodynamic path angle as a singular control. This leads to a model that is singular on both control elements. Followed by a theorem, we present a compact closed-form solution for the multi-control singular model in the form of Jacobian compositions through the Pontryagin Maximum Principle. The optimal structure is dependent on the boundaries as well as the relaxed parameters involved. An algorithm is proposed to capture various combinations of bang and singular extremals for the control elements, leading to some new optimal structures, as will be shown through the case study. Results due to the singular model are compared with the solutions due to the original model with the overall conclusion of extreme accuracy. Finally, the paper terminates with a discussion on the merits of the singular solutions in terms of computational time and accuracy.

Keywords: Indirect Optimization; Optimal Control; Aircraft Trajectory Optimization; Closed Form Solutions; Pure Singular Model v.s. Complete Model

1 Introduction

The aerospace industries are inquisitively in demand of modern optimization tools to minimize the total flight cost. The cost is usually a combination of the arrival time, fuel burn together with some environmental hazards such as climate and noise.

Aircraft trajectory optimization as an Optimal Control Problem (OCP) has been the target of many research centers. The solution for this class of OCPs has been sought through the well-posed optimization methods; i.e., mathematical parameter optimization, heuristic parameter optimization, Pontyagin Maximum Principle, PMP, and dynamic programming (in approximate or classic form). Let us refer the mathematical parameter optimization as the direct mathematical (gradient-based) method or in short, the direct method and PMP as the indirect method, being two counterpart mathematical methods in optimization theory.

*Corresponding Author. Email: ajafarim@pa.uc3m.es, Tel.: +34 666 251 627.

Due to the complexity and sensitivity of the resulting multiplier system from PMP, the indirect method shares the least contribution among the rest in aircraft trajectory optimization (see [1]). This complexity, by itself, has drawn researchers to the direct methods as well as the heuristic methods with limited level of accuracy and warrant.

The direct method usually prevails in the matter of labor with a competing level of accuracy compared to its counterpart indirect method. The multipliers in a direct method imitate the presence of co-state dynamics through Karush-Kuhn-Tucker (KKT) conditions, which explains the accuracy of direct methods. Therefore, mathematically speaking, the direct method is a discrete version of PMP in such a way that the solutions from the direct method correspond to counterpart indirect solutions and the correspondence is regarded as the Covector Mapping Principle (CMP), a lemma, initially postulated by Ross ([2], [3]). For this reason, the direct solutions are sometimes regarded as the numerical solutions, whereas the indirect solutions are the analytic ones, the terminologies used throughout this paper as well.

The goal of the present research is to develop a mathematical framework to solve a general version of the commercial aircraft trajectory optimization problem in a vertical plane. Relying on the physics of the problem, we initially derive a corresponding singular model, featured by two singular control elements, an arbitrary objective function, spatial wind field as well as equality and inequality constraints. Next, we develop a mathematical framework to compute the co-state dynamics and the singular controls in matrix form. The mathematical framework is accompanied by an algorithm that bypasses the irregularity issue within the co-state system through a recursive sequence. Finally, we compare the analytical solutions to the numerical solutions (due to the non-reduced model) to show that both coincide perfectly.

In line with the scope of the present work, we give a review of the previous analytical works on aircraft trajectory optimization (those with the vertical plane hypothesis) and explicate the major gap in the literature.

Ardema solved the minimum time aircraft trajectory in the climb phase by the principle of singular perturbation, presumably for the first time (see [4]). Particularly, in [4], the minimum time problem has been viewed as a singular perturbation which is due to the existence of fast and slow variables within the system dynamics. More recently, in [5], an analogous minimum time problem has been solved with mass evolution; however, with no relaxed parameters, constraints, or wind consideration. The significant outcome of [5] is that the singular minimum time solution can be considered a highly accurate solution for the original problem without simplification. Moreover, the singular solution (as found in [5]) is in the form of bang-singular-bang (BSB). In [6], the author has presented a detailed singular solution for the minimum time problem with wind considerations, however, the evolution of mass has been ignored. In [7], the singular minimum fuel aircraft trajectory optimization has been solved for the main flight phases, i.e., climb, cruise and descent. Specifically, in each phase, the authors have assumed the control as a single input variable together with some matching criteria. In [7], the optimal solutions have been sought in the form of BSB for all the studied cases. In [8] authors have presented a singular solution for a simplified un-powered descent problem with a cost resembling the environmental emission impact. The indirect solutions in [8] have been (partially) compared with those from a direct collocation method for the same simplified OCP and a very good agreement has been acknowledged. It is worth mentioning that the un-powered descent model in [8] includes inequality constraints on the state vector and the scalar control (aerodynamic path angle). In [9], the singular maximum range aircraft trajectory optimization in the cruise phase has been solved. Specifically, for simplified system dynamics, authors have derived the singular extremal by Green's theorem ([10] and [11]) which applies to a singular OCP with two state variables. In [12] and [13], authors have extended the previous work, [9], by accounting for the compressibility effect as well as fixed arrival time in a cruise phase. In [14], authors have presented solutions for a 2D aircraft trajectory optimization (vertical plane) in the climbing phase with cost being a combination of time and fuel consumption, however, for some limited range of the parameters involved and with no wind consideration. More specifically, in [14], a direct method has been employed for the initialization of the multipliers associated with the PMP model. In this view, the solution procedure in [14] is a hybrid approach. In [15], the minimum fuel cruise phase problem with a fixed arrival time in the presence of an average wind

field is solved. In [15], the optimal structure is sought through BSB for the scalar control, and throttle setting. In [16] authors have solved the maximum range un-powered descent problem with the aerodynamic path angle being the scalar control under the assumption of BSB optimality. The relaxed parameters in [16] are the aircraft's initial weight as well as the wind parameter.

In short, all the previous analytical works on aircraft flights (optimization in a vertical plane) address the problem with one active singular control on a case-by-case basis and in this respect, there is no analytical work considering two active singular controls. In other words, the other (possibly) singular control appearing in the problem has been prefixed as a trivially-bang solution in the previous works. Here, we show that for a given flight phase, the other singular control may switch. Besides, the BSB structure may not always be the optimal structure. Apart from the structure of the singular solution, from the available literature, there seems to be no detailed comparison between the optimal solutions due to the reduced singular model and those from the non-reduced model. This gap is also replenished in this work.

In principle, the appearance of several singular controls complicates the solution procedure. In this respect, analytical works on OCPs with several singular controls are limited in the area of optimal control. For this, we address to [17], [18], [19] and [20]. More specifically, in [17] and [18], the collision avoidance OCP is tackled analytically. The OCP in [17] and [18] is a singular dual-control OCP and authors have shown that the two controls cannot be singular simultaneously. Similarly, combination therapy for tumors has been formulated as an OCP with two active singular controls in [19] and [20]. In [20], authors have rejected the possibility of a singular surface and in [19], authors have used the argument for a more complex model and conjectured, based on observations, that the singular surface is not a case of optimality.

We construct the paper by first defining the original aircraft trajectory optimization model in a vertical plane($\mathcal{P}^{(1)}$) and the corresponding singular model ($\mathcal{P}^{(2)}$) in Sec. 2. The novel contributions of the present paper have been organized as:
1) In Sec.3, presenting a compact closed-form solution in form of Jacobian compositions for $\mathcal{P}^{(2)}$ with full dynamics, two active singular control elements (aerodynamic path angle and throttle setting), spatial wind field, arbitrary objective as well as equality and inequality constraints (the closed-form solution can be computed easily in any platform supporting symbolic calculations such as MATLAB).
2) In Sec.3 (Appendix A), detailed insights to the closed-form solution through matrix analysis.
3) In Sec.4, presenting an effective algorithm to capture various combinations of bang and singular extremals and the possible switches inside or outside the singular arcs (the algorithm circumvents the irregularity issue within the co-state system).
4) In Sec.5, solving an example of partial climb phase with full dynamics, equality and inequality constraints, wind field as well as two active singular control elements and the objective being a combination of arrival time and fuel burn (this cost function is also new in view of the analytical aircraft trajectory optimization).
5) In Subsec.5.2.3, showing that the optimal aerodynamic path angle may follow structures other than BSB, i.e., Bang-Singular-Bang-Bang (BSBB) and asymptotic Bang-Bang (aBB).
6) Subsec.5.2.4, showing that for a pure climb phase, the optimal throttle setting may switch and a preset trivial bang structure is not optimal.
7) In Subsec.5.2.1-5.2.5, comparing the solutions from $\mathcal{P}^{(2)}$ with those due to $\mathcal{P}^{(1)}$.

2 Problem Statement

In this section, we introduce the aircraft trajectory optimization problem in a vertical plane (original model, $\mathcal{P}^{(1)}$). The singular model (reduced model, $\mathcal{P}^{(2)}$) is presented afterwards. The singular model is a reduced model through applying singular perturbation of the zeroth order, [21], and order of magnitude analysis in accordance with the physics of a commercial aircraft.

2.1 Aircraft Trajectory Optimization Problem in a Vertical Plane (Original Model, $\mathcal{P}^{(1)}$)

The problem can be formulated as an OCP through the following Bolza form ([22], [23]):

$$\min_{U:=[\Pi(t),C_l(t)]^T} \mathcal{J} = \int_0^{t_f} \mathcal{L}(x,h,v,\Pi)dt \tag{1}$$

Subject to:

$$\begin{aligned}
&\frac{dx}{dt} = v\cos\gamma + w(x,h)\\
&\frac{dh}{dt} = v\sin\gamma\\
&\frac{dv}{dt} = \frac{\Pi T(v,h)\cos\epsilon - D(m,v,h)}{m} - g\sin\gamma - \left(\frac{\partial w}{\partial x}\left(v\cos\gamma + w\right) + \frac{\partial w}{\partial h}v\sin\gamma\right)\cos\gamma\\
&\frac{dm}{dt} = -\Pi C_s(v,h)T(v,h)\\
&\frac{d\gamma}{dt} = \frac{\Pi T(v,h)\sin\epsilon + L(m,v,h)}{mv} - \frac{g}{v} + \left(\frac{\partial w}{\partial x}\left(v\cos\gamma + w\right) + \frac{\partial w}{\partial h}v\sin\gamma\right)\frac{\sin\gamma}{v}\\
&\gamma_{min} \le \gamma \le \gamma_{max} \quad \Pi_{min} \le \Pi \le \Pi_{max}\\
&V_{CAS,min} \le V_{CAS} \le V_{CAS,max} \quad M_{min} \le M \le M_{max}
\end{aligned} \tag{2}$$

In Eq. (2), $x(t)$ is the tangential coordinate (horizontal distance traveled), $h(t)$ is the normal coordinate (altitude), v is the aerodynamic speed, $\gamma(t)$ is the aerodynamic path angle, $\Pi(t)$ is the throttle setting, $m(t)$ is the aircraft mass, w is the horizontal wind field, D is the aerodynamic drag, T is the thrust force, ϵ is the thrust angle of attack (which is assumed to be zero), L is the aerodynamic lift defined as: $L = \frac{1}{2}C_l\rho(h)sv^2$, C_s is the fuel flow, g is the gravitational acceleration, C_l is the lift coefficient and t is time. Moreover, V_{CAS} and $Mach$ number are defined as:

$$V_{CAS} := \sqrt{\frac{2P_0}{\mu^*\rho(0)}\left(\left(\frac{P(h)}{P_0}\left(\left(\frac{\mu^* v^2}{2R\Theta(h)} + 1\right)^{\frac{1}{\mu^*}} - 1\right) + 1\right)^{\mu^*} - 1\right)} \tag{3}$$

$$M := \frac{v}{\sqrt{\gamma^* R\Theta(h)}} \tag{4}$$

The horizontal wind field is a steady-state flow and is a function of coordinates x and h. Moreover, the cost functional is relaxed, convertible to various forms such as minimum time, maximum distance traveled, minimum fuel, as well as minimum environmental impacts or a combination of these terms.

$\mathcal{P}^{(1)}$ is an OCP with constraints on state and control vectors. In addition, the OCP is singular on $\Pi(t)$ and regular on $C_l(t)$.

2.2 Commercial Aircraft Trajectory Optimization Problem in a Vertical Plane (Reduced Model, $\mathcal{P}^{(2)}$)

For a commercial aircraft, the significant time scale separation makes it possible to apply the singular perturbation technique:

$$p\frac{d\gamma}{dt} = \frac{\Pi T(v,h)\sin\epsilon + L(m,v,h)}{mv} - \frac{g}{v} + \left(\frac{dw}{dx}\left(v\cos\gamma + w\right) + \frac{dw}{dh}v\sin\gamma\right)\frac{\sin\gamma}{v} \tag{5}$$

In Eq. (5), p is a perturbation parameter. The zeroth term is linked to $p = 0$.

Now, we apply order of magnitude analysis to determine the significance of the terms involved. For this, we note that Eq. (5) is significant in climb or descent phases. Therefore, it is reasonable to take the following orders for the involved variables: $\sin\gamma \equiv O(10^{-1})$ ($\cos\gamma \equiv O(1)$), $v \equiv O(10^2)$, $\Delta w \equiv O(10)$ ($w \equiv O(10)$), $\Delta x \equiv O(10^5)$, $\Delta h \equiv O(10^3)$ and $g \equiv O(1)$. Moreover, we set $\epsilon = 0$.

With the above orders, the last term in Eq. (5) is negligible through the following analysis:

$$O\left(\| \frac{\Delta w}{\Delta x}\sin\gamma\cos\gamma + w\frac{\Delta w}{\Delta x}\frac{\sin\gamma}{v} + \frac{\Delta w}{\Delta h}\sin^2\gamma \|_1\right) \equiv O(10^{-4}) << O(\frac{g}{v}) = O(10^{-2}) \tag{6}$$

Therefore, the last term in Eq. (5) can be canceled, leaving:

$$C_l \approx \frac{2mg}{\rho(h)sv^2} \tag{7}$$

Plugging Eq. (7) into Eq. (2), together with $\epsilon = 0$ and $\gamma(t) << 1$, $\mathcal{P}^{(1)}$ turns into the singular model, $\mathcal{P}^{(2)}$:

$$\min_{\gamma(t),\Pi(t)} \mathcal{J} = \int_0^{t_f} \mathcal{L}(x,h,v,\Pi)dt \tag{8}$$

Subject to:

$$\begin{aligned}
&\frac{dx}{dt} = v + w(x,h)\\
&\frac{dh}{dt} = v\gamma\\
&\frac{dv}{dt} = \frac{\Pi T(v,h) - D(m,v,h)}{m} - g\gamma - \frac{\partial w}{\partial x}(v+w) - \frac{\partial w}{\partial h}v\gamma\\
&\frac{dm}{dt} = -\Pi C_s(v,h)T(v,h)\\
&\gamma_{min} \le \gamma \le \gamma_{max} \quad \Pi_{min} \le \Pi \le \Pi_{max}\\
&V_{CAS,min} \le V_{CAS} \le V_{CAS,max} \quad M_{min} \le M \le M_{max}
\end{aligned} \tag{9}$$

$\mathcal{L}$ is linearly dependent on Π if the cost functional contains the minimum fuel term. Therefore, in general, this is a singular OCP on both control elements, $\Pi(t)$ and $\gamma(t)$.

3 Closed-Form Solution for $\mathcal{P}^{(2)}$

In this section, we initially present $\mathcal{P}^{(2)}$ in vector form. Then, through theorem 1 we show that in the case that the state inequality constraints are inactive, a singular surface does not exist. The elements of the closed-form solution are specified through a schematic (Fig. 1). In subsection 3.1 and 3.2 these elements are found in the form of Jacobian compositions. In subsection 3.3 we give complementary theorems to deal with the continuity of the co-state variables.

In vector form, $\mathcal{P}^{(2)}$ can be recast as:

$$\min_{U(t)} \mathcal{J} = \int_0^{t_f} \mathcal{L}(X,U)dt \tag{10}$$

Subject to:

$$\begin{aligned}
&\frac{dX}{dt} = F(X,U)\\
&\mathcal{C}(U) \le 0\\
&\mathcal{S}(X) \le 0\\
&\phi_0(X_0) = X_0 - X(0) = 0, \quad \phi_0 \in \mathbb{R}^4\\
&\phi_f(X_f) = X_f - X(t_f) = 0, \quad \phi_f \in \mathbb{R}^q, q \le 4
\end{aligned} \tag{11}$$

Where:

$$\begin{aligned} X &= [x, h, v, m]^T \\ F &= [F_1, F_2, F_3, F_4]^T \\ U &= [\gamma, \Pi]^T \end{aligned} \tag{12}$$

In addition:

$$\begin{aligned} \mathcal{C}(U) &= [\gamma - \gamma_{max}, \gamma_{min} - \gamma, \Pi - \Pi_{max}, \Pi_{min} - \Pi]^T \\ \mathcal{S}(X) &= [V_{CAS} - V_{CAS,max}, V_{CAS,min} - V_{CAS}, M - M_{max}, M_{min} - M]^T \end{aligned} \tag{13}$$

Together with:

$$\begin{aligned} F_1 &= v + w \\ F_2 &= v\gamma(t) \\ F_3 &= \frac{\Pi(t)T - D}{m} - \frac{dw}{dx}(v + w) - (g + v\frac{dw}{dh})\gamma(t) \\ F_4 &= -\Pi(t)C_sT \end{aligned} \tag{14}$$

The augmented cost is:

$$\begin{aligned} &\bar{\mathcal{J}} = \nu_0^T \phi_0(X_0) + \nu_f^T \phi_f(X_f) + \\ &\int_0^{t_f} \Big(\mathcal{L}(X, U) + \lambda^T(t)\big(F(X, U) - \frac{d}{dt}X\big) + \mu^T(t)\mathcal{C}(U) + \eta^T(t)\mathcal{S}(X) \Big) dt \end{aligned} \tag{15}$$

Where, $\lambda(t) = [\lambda_x(t), \lambda_h(t), \lambda_v(t), \lambda_m(t)]^T$, $\mu(t) = [\mu(t)_U^\gamma, \mu(t)_L^\gamma, \mu(t)_U^\Pi, \mu(t)_L^\Pi]^T$, $\nu_0 \in \mathbb{R}^4$ and $\nu_f \in \mathbb{R}^q$ are the scalar multipliers associated with the boundary conditions. Moreover, $\eta(t) \in \mathbb{R}^4$ is the multiplier vector for the state inequality constraint.

The Hamiltonian, associated with Eq. (15), is:

$$\mathcal{H}(t) = \mathcal{L}(X, U) + \lambda^T F(X, U) + \mu^T \mathcal{C}(U) + \eta^T \mathcal{S}(X) \tag{16}$$

The PMP optimality conditions are:

$$\begin{aligned} &\frac{\partial \mathcal{H}}{\partial U} = 0 \\ &\mu^T \mathcal{C} = 0 \quad \mu \geq 0 \\ &\eta^T \mathcal{S} = 0 \quad \eta \geq 0 \end{aligned} \tag{17}$$

The co-state dynamics and the transversality conditions are:

$$\begin{aligned} &\frac{d\lambda^T}{dt} = -\frac{\partial \mathcal{H}}{\partial X} \\ &\lambda_0 = \lambda(0) = -\Big(\frac{\partial \phi_0}{\partial X_0}\Big)^T \nu_0 \\ &\lambda_f = \lambda(t_f) = -\Big(\frac{\partial \phi_f}{\partial X_f}\Big)^T \nu_f \\ &\mathcal{H}_f = \mathcal{H}(t_f) = -\nu_f^T \frac{\partial \phi_f}{\partial t_f} = 0 \end{aligned} \tag{18}$$

The system is autonomus. Therefore, along the optimality we have:

$$\mathcal{H}(t) = Constant, \quad t \in [0, t_f] \tag{19}$$

Eq. (19), together with the Hamiltonian condition in Eq. (18), gives:

$$\mathcal{H}(t) = 0, \quad t \in [0, t_f] \tag{20}$$

Using Eq. (16) and Eq. (17), the optimality conditions become:

$$\frac{\partial \mathcal{H}}{\partial \gamma} = \lambda^T \frac{\partial F}{\partial \gamma} + \mu_U^{\gamma}(t) - \mu_L^{\gamma}(t) = 0 \tag{21}$$

$$\frac{\partial \mathcal{H}}{\partial \Pi} = \frac{\partial \mathcal{L}}{\partial \Pi} + \lambda^T \frac{\partial F}{\partial \Pi} + \mu_U^{\Pi}(t) - \mu_L^{\Pi}(t) = 0 \tag{22}$$

Since the Hamiltonian is linear on $\gamma(t)$ and $\Pi(t)$, the optimal solution is either singular or bang for each. Therefore:

$$\gamma^*(t) = \begin{cases} \gamma_{min} & \lambda^T \frac{\partial F}{\partial \gamma} - \mu_L^{\gamma}(t) = 0 \\ \gamma_{max} & \lambda^T \frac{\partial F}{\partial \gamma} + \mu_U^{\gamma}(t) = 0 \\ \gamma_s(t) & \lambda^T \frac{\partial F}{\partial \gamma} = 0 \end{cases} \tag{23}$$

$$\Pi^*(t) = \begin{cases} \Pi_{min} & \frac{\partial K}{\partial \Pi} + \lambda^T \frac{\partial F}{\partial \Pi} - \mu_L^{\Pi}(t) = 0 \\ \Pi_{max} & \frac{\partial K}{\partial \Pi} + \lambda^T \frac{\partial F}{\partial \Pi} + \mu_U^{\Pi}(t) = 0 \\ \Pi_s(t) & \frac{\partial K}{\partial \Pi} + \lambda^T \frac{\partial F}{\partial \Pi} = 0 \end{cases} \tag{24}$$

Let us define switching functions as, $S^{\gamma}(t) = \lambda^T \frac{\partial F}{\partial \gamma}$ and $S^{\Pi}(t) = \frac{\partial \mathcal{L}}{\partial \Pi} + \lambda^T \frac{\partial F}{\partial \Pi}$. Therefore, Eq. (23) and Eq. (24) can be written in the following forms:

$$\gamma^*(t) = \begin{cases} \gamma_{min} & S^{\gamma}(t) = \mu_L^{\gamma}(t) > 0 \\ \gamma_{max} & S^{\gamma}(t) = -\mu_U^{\gamma}(t) < 0 \\ \gamma_s(t) & S^{\gamma}(t) = 0 \end{cases} \tag{25}$$

$$\Pi^*(t) = \begin{cases} \Pi_{min} & S^{\Pi}(t) = \mu_L^{\Pi}(t) > 0 \\ \Pi_{max} & S^{\Pi}(t) = -\mu_U^{\Pi}(t) < 0 \\ \Pi_s(t) & S^{\Pi}(t) = 0 \end{cases} \tag{26}$$

In order to obtain $\gamma_s(t)$ and $\Pi_s(t)$, we re-write the present affine system as:

$$F = \bar{F} + \gamma(t) F_{s,\gamma} + \Pi(t) F_{s,\Pi} \tag{27}$$

In Eq. (27), $\bar{F}$, $F_{s,\gamma}$ and $F_{s,\Pi}$ are:

$$\begin{aligned} \bar{F} &= [\bar{F}_1, \bar{F}_2, \bar{F}_3, \bar{F}_4]^T \\ F_{s,\gamma} &= [F_{s1,\gamma}, F_{s2,\gamma}, F_{s3,\gamma}, F_{s4,\gamma}]^T \\ F_{s,\Pi} &= [F_{s1,\Pi}, F_{s2,\Pi}, F_{s3,\Pi}, F_{s4,\Pi}]^T \end{aligned} \tag{28}$$

With the vectors' elements:

$$\begin{aligned} &\bar{F}_1 = v + w, \quad \bar{F}_2 = 0, \quad \bar{F}_3 = -\frac{D}{m} - \frac{\partial w}{\partial x}(v + w), \quad \bar{F}_4 = 0 \\ &F_{s1,\gamma} = 0, \quad F_{s2,\gamma} = v \quad F_{s3,\gamma} = -g - v\frac{\partial w}{\partial h}, \quad F_{s4,\gamma} = 0 \\ &F_{s1,\Pi} = 0, \quad F_{s2,\Pi} = 0 \quad F_{s3,\Pi} = \frac{T}{m}, \quad F_{s4,\Pi} = -C_s T \end{aligned} \tag{29}$$

Therefore, the Hamiltonian can be recast as:

$$\mathcal{H} = \mathcal{L} + \lambda^T \bar{F} + \gamma \lambda^T F_{s,\gamma} + \Pi \lambda^T F_{s,\Pi} + \mu^T \mathcal{C} + \eta^T \mathcal{S} \tag{30}$$

Theorem 1. *In the case that the state inequality constraints are inactive, i.e., $\eta = 0$, there is no time interval over which the control elements are both singular.*

Proof. By contradiction, assume that there exists an interval $t \in [t_a, t_b]$ such that the control elements are both singular. This means,

$$\mathcal{H} = \frac{\partial \mathcal{H}}{\partial \gamma} = \frac{\partial \mathcal{H}}{\partial \Pi} = \frac{d}{dt}\frac{\partial \mathcal{H}}{\partial \gamma} = \frac{d}{dt}\frac{\partial \mathcal{H}}{\partial \Pi} = \frac{d^2}{dt^2}\frac{\partial \mathcal{H}}{\partial \gamma} = \frac{d^2}{dt^2}\frac{\partial \mathcal{H}}{\partial \Pi} = 0, \quad \mu = \eta = 0, \quad t \in [t_a, t_b] \tag{31}$$

By assuming $\mathcal{L} = \bar{\mathcal{L}} + \Pi(t)\mathcal{L}_{s,\Pi}$, we have:

$$\begin{aligned}
&\mathcal{H} = \bar{\mathcal{L}} + \lambda^T \bar{F} = 0, \quad \frac{\partial \mathcal{H}}{\partial \gamma} = \lambda^T F_{s,\gamma} = S^\gamma = 0 \\
&\frac{\partial \mathcal{H}}{\partial \Pi} = \mathcal{L}_{s,\Pi} + \lambda^T F_{s,\Pi} = S^\Pi = 0, \quad \frac{d}{dt}\frac{\partial \mathcal{H}}{\partial \gamma} = \frac{dS^\gamma}{dt} = 0 \\
&\frac{d^2}{dt^2}\frac{\partial \mathcal{H}}{\partial \gamma} = \frac{d^2 S^\gamma}{dt^2} = 0, \quad \frac{d}{dt}\frac{\partial \mathcal{H}}{\partial \Pi} = \frac{dS^\Pi}{dt} = 0 \\
&\frac{d^2}{dt^2}\frac{\partial \mathcal{H}}{\partial \Pi} = \frac{d^2 S^\Pi}{dt^2} = 0
\end{aligned} \tag{32}$$

From the co-state dynamics, Eq.(18):

$$\frac{d\lambda^T}{dt} = -\frac{\partial \mathcal{L}}{\partial X} - \lambda^T \frac{\partial \bar{F}}{\partial X} - \gamma(t)\lambda^T \frac{\partial F_{s,\gamma}}{\partial X} - \Pi(t)\lambda^T \frac{\partial F_{s,\Pi}}{\partial X} \tag{33}$$

Plugging Eq. (33) into (32), one ends up with 7 independent algebraic equations for defining the optimality with 6 unknowns, i.e., $\lambda \in \mathbb{R}^4$ plus $\gamma_s(t)$ and $\Pi_s(t)$. Therefore, the algebraic system is inconsistent and the proof is complete. □

Some Definitions:
1) Singular extremal: an interval over which at least one control element is singular.
2) Over the singular extremal: $U_s := P(X, \lambda_s^T)$.
3) Over the singular extremal: $\lambda_s^T := G(X, \lambda_x)$.
4) Switching point: a time instant at which at least one control element changes its structure.

There is a possibility that U_s has no dependency on λ_s^T. In this situation, the solution procedure is simplified by removing the loop processing. However, in a more general manner (including the present case study in Sec.5), the loop processing is unavoidable.

The closed-form solution for $\mathcal{P}^{(2)}$ includes finding two significant operators, G and P. With G and P found, it is possible to solve over the singular extremal. In this sense, we may suppose that the optimal solution contains a singular arc (U_s) between two switching points, $s^{(k)}$ and $s^{(k+1)}$. In this situation, we can solve for $t_i \in [s^{(k)}, s^{(k+1)}]$. Fig. 1 shows this procedure in schematic. In the following subsections, we find these operators in closed-forms.

3.1 γ-Singular Scenario

There is an interval, $t \in [t_a, t_b]$ such that $\gamma(t)$ is singular. Therefore, from theorem 1, $\Pi(t)$ must be bang with possible switching instants, i.e., $\Pi(t) = \Pi_b := \Pi_{max} \vee \Pi_{min}$.

For this case, the optimality conditions are:

$$\mathcal{L} + \lambda^T \bar{F} + \Pi_b \lambda^T F_{s,\Pi} = 0, \quad S^\gamma(t) = \lambda^T F_{s,\gamma} = 0, \quad \frac{dS^\gamma}{dt} = \frac{d(\lambda^T F_{s,\gamma})}{dt} = 0 \tag{34}$$

In Eq. (34), $\mathcal{L} = \mathcal{L}(X, \Pi_b) = \bar{\mathcal{L}} + \Pi_b \mathcal{L}_{s,\Pi}$. The co-state dynamics are:

$$\frac{d\lambda^T}{dt} = -\frac{\partial \mathcal{L}}{\partial X} - \lambda^T \frac{\partial \bar{F}}{\partial X} - \gamma(t)\lambda^T \frac{\partial F_{s,\gamma}}{\partial X} - \Pi_b \lambda^T \frac{\partial F_{s,\Pi}}{\partial X} - \eta^T \frac{\partial \mathcal{S}}{\partial X} \tag{35}$$

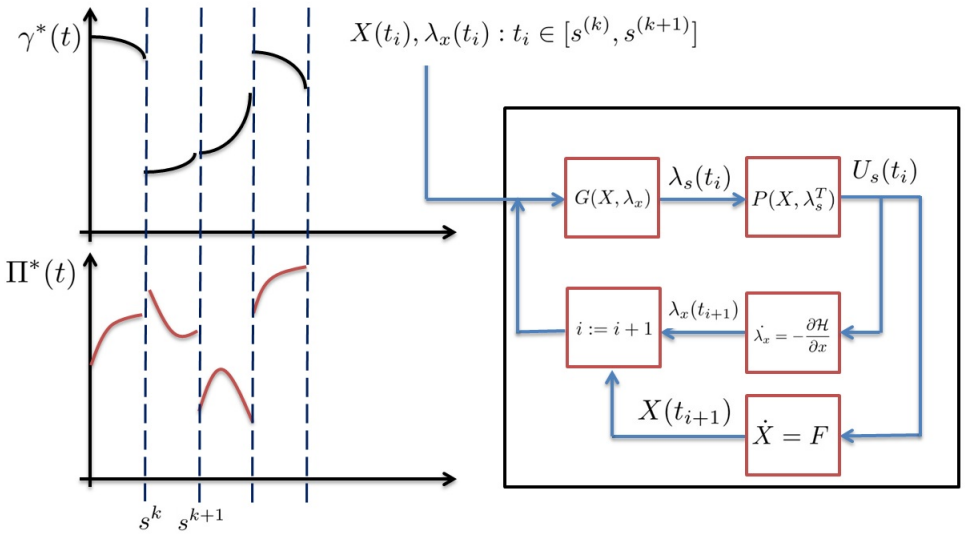

Figure 1: Solution procedure over the singular extremal using the closed-form operators, G and P

Let us initially assume that the state inequality constrains are inactive, i.e., $\eta = 0$. Therefore:

$$\begin{aligned} &\frac{dS^\gamma}{dt} = \frac{d\lambda^T}{dt} F_{s,\gamma} + \lambda^T \frac{dF_{s,\gamma}}{dt} = \\ &- \left(\frac{\partial \mathcal{L}}{\partial X} + \lambda^T \frac{\partial \bar{F}}{\partial X} + \gamma(t) \lambda^T \frac{\partial F_{s,\gamma}}{\partial X} + \Pi_b \lambda^T \frac{\partial F_{s,\Pi}}{\partial X}\right) F_{s,\gamma} + \lambda^T \frac{\partial F_{s,\gamma}}{\partial X} F \end{aligned} \tag{36}$$

Plugging Eq. (27) into Eq. (36), $\gamma(t)$ is canceled out and the algebraic system, in Jacobian form, defining the co-state dynamics become:

$$\mathcal{L} + \lambda^T (\bar{F} + \Pi_b F_{s,\Pi}) = 0 \tag{37}$$

$$\lambda^T F_{s,\gamma} = 0 \tag{38}$$

$$\lambda^T \left(\mathbf{J}[F_{s,\gamma}](\bar{F} + \Pi_b F_{s,\Pi}) - \mathbf{J}[\bar{F} + \Pi_b F_{s,\Pi}] F_{s,\gamma} \right) - \frac{\partial \mathcal{L}}{\partial X} F_{s,\gamma} = 0 \tag{39}$$

In Eq. (39), $\mathbf{J}[\bullet]$ is the Jacobian:

$$\mathbf{J}[\Xi(X)] = \frac{\partial (\Xi_1, ..., \Xi_L)}{\partial (X_1, ..., X_L)} \tag{40}$$

We solve Eq. (37), Eq. (38) and Eq. (39) for λ_h, λ_v and λ_m, that is:

$$\begin{pmatrix} \lambda_h \\ \lambda_v \\ \lambda_m \end{pmatrix} = M^{-1} R =: G^{\gamma_s} \tag{41}$$

In Eq. (41):

$$M = \begin{pmatrix} \bar{F}_2 + \Pi_b F_{s2,\Pi} & \bar{F}_3 + \Pi_b F_{s3,\Pi} & \bar{F}_4 + \Pi_b F_{s4,\Pi} \\ F_{s2,\gamma} & F_{s3,\gamma} & F_{s4,\gamma} \\ \mathcal{A}_2 & \mathcal{A}_3 & \mathcal{A}_4 \end{pmatrix} \tag{42}$$

and,

$$R = \begin{pmatrix} -\mathcal{L} - \lambda_x (\bar{F}_1 + \Pi_b F_{s1,\Pi}) \\ -\lambda_x F_{s1,\gamma} \\ -\lambda_x \mathcal{A}_1 + \frac{\partial \mathcal{L}}{\partial X} F_{s,\gamma} \end{pmatrix} \tag{43}$$

The vector, $\mathcal{A}$, is the same as the commutativity of the vector functions in Lie bracket notation (see [14]):

$$\mathcal{A} = \mathbf{J}[F_{s,\gamma}](\bar{F} + \Pi_b F_{s,\Pi}) - \mathbf{J}[\bar{F} + \Pi_b F_{s,\Pi}]F_{s,\gamma} = [\mathcal{A}_1, \mathcal{A}_2, \mathcal{A}_3, \mathcal{A}_4]^T \tag{44}$$

$\gamma_s(t)$ is linked to the solution of:

$$\frac{d^2 S^\gamma}{dt^2} = \frac{d^2\big(\lambda^T F_{s,\gamma}\big)}{dt^2} = 0 \tag{45}$$

Eq. (45) can be expanded as:

$$\frac{d\lambda^T}{dt}\mathcal{A} + \lambda^T \frac{d\mathcal{A}}{dt} - \frac{d}{dt}\big(\frac{\partial \mathcal{L}}{\partial X}\big)F_{s,\gamma} - \frac{\partial \mathcal{L}}{\partial X}\frac{dF_{s,\gamma}}{dt} = 0 \tag{46}$$

The time derivatives of $\frac{\partial \mathcal{L}}{\partial X}$ and $\mathcal{A}$ are:

$$\begin{aligned} &\frac{d}{dt}\frac{\partial \mathcal{L}}{\partial X} = F^T \mathbf{J}[\big(\frac{\partial \mathcal{L}}{\partial X}\big)^T]^T = F^T \mathbf{J}[\big(\frac{\partial \mathcal{L}}{\partial X}\big)^T] \\ &\frac{d\mathcal{A}}{dt} = \mathbf{J}[\mathcal{A}]F \end{aligned} \tag{47}$$

Eq. (46), together with Eq. (27) and Eq. (47), gives:

$$\gamma_s(t) = \frac{\lambda^T\Big(\mathbf{J}[\bar{F} + \Pi_b F_{s,\Pi}]\mathcal{A} - \mathbf{J}[\mathcal{A}](\bar{F} + \Pi_b F_{s,\Pi})\Big) + T_1}{\lambda^T\Big(\mathbf{J}[\mathcal{A}]F_{s,\gamma} - \mathbf{J}[F_{s,\gamma}]\mathcal{A}\Big) + T_2} =: P^{\gamma_s} \tag{48}$$

In Eq. (47), T_1 and T_2 are:

$$T_1 = \frac{\partial \mathcal{L}}{\partial X}\mathcal{A} + \frac{\partial \mathcal{L}}{\partial X}\mathbf{J}[F_{s,\gamma}](\bar{F} + \Pi_b F_{s,\Pi}) + (\bar{F} + \Pi_b F_{s,\Pi})^T \mathbf{J}[\big(\frac{\partial \mathcal{L}}{\partial X}\big)^T]F_{s,\gamma} \tag{49}$$

$$T_2 = -\frac{\partial \mathcal{L}}{\partial X}\mathbf{J}[F_{s,\gamma}]F_{s,\gamma} - F_{s,\gamma}^T \mathbf{J}[\big(\frac{\partial \mathcal{L}}{\partial X}\big)^T]F_{s,\gamma} \tag{50}$$

For a non-saturating singular control, the generalized Clebsch (Legendre) condition ([24]) for the present OCP is equivalent to:

$$-\frac{\partial}{\partial \gamma}\frac{d^2 S^\gamma}{dt^2} = -\lambda^T\Big(\mathbf{J}[\mathcal{A}]F_{s,\gamma} - \mathbf{J}[F_{s,\gamma}]\mathcal{A}\Big) - T_2 \geq 0 \tag{51}$$

In the case that the state inequality constraints are active, i.e., $\eta \neq 0$, it can be assumed an interval, $[t_c, t_d] \subseteq [t_a, t_b]$ such that at least on element of $\mathcal{S}$ is zero; i.e., $\mathcal{S}_a = 0$. Therefore, for $t \in [t_c, t_d]$:

$$\mathcal{S}_a = \frac{d\mathcal{S}_a}{dt} = 0 \tag{52}$$

From $\frac{d\mathcal{S}_a}{dt} = 0$:

$$\gamma_{s,a}(t) = -\frac{\big(\frac{\partial \mathcal{S}_a}{\partial X}\big)\big(\bar{F} + \Pi_b F_{s,\Pi}\big)}{\big(\frac{\partial \mathcal{S}_a}{\partial X}\big)F_{s,\gamma}} =: P^{\gamma_{s,a}} \tag{53}$$

Since, we are necessarily in the singular arc territory, the following holds:

$$\eta_a = \frac{\lambda^T \mathcal{A} - \frac{\partial \mathcal{L}}{\partial X}F_{s,\gamma}}{\frac{\partial \mathcal{S}_a}{\partial X}F_{s,\gamma}} \tag{54}$$

For $t \in [t_c, t_d]$ we have, $\gamma_s = \gamma_{s,a}$. Therefore, η_a can be determined in terms of the state variables and λ_x through the time derivative of Eq. (54). However, this derivation is omitted since the value of η_a is out of necessity and $\gamma_{s,a}$ suffices to process the integration.

3.2 Π-Singular Scenario

There is an interval, $t \in [t_{a'}, t_{b'}]$ such that $\Pi(t)$ is singular. Therefore, from theorem 1, $\gamma(t)$ must be bang with possible switching instants, i.e., $\gamma(t) = \gamma_b := \gamma_{max} \vee \gamma_{min}$.

For this case, the optimality conditions are:

$$\bar{\mathcal{L}} + \lambda^T \bar{F} + \gamma_b \lambda^T F_{s,\gamma} = 0, \quad S^{\Pi}(t) = \mathcal{L}_{s,\Pi} + \lambda^T F_{s,\Pi} = 0, \quad \frac{dS^{\Pi}}{dt} = \frac{d\big(\mathcal{L}_{s,\Pi} + \lambda^T F_{s,\Pi}\big)}{dt} = 0 \tag{55}$$

The co-state dynamics are:

$$\frac{d\lambda^T}{dt} = -\frac{\partial \mathcal{L}}{\partial X} - \lambda^T \frac{\partial \bar{F}}{\partial X} - \gamma_b \lambda^T \frac{\partial F_{s,\gamma}}{\partial X} - \Pi(t) \lambda^T \frac{\partial F_{s,\Pi}}{\partial X} - \eta^T \frac{\partial \mathcal{S}}{\partial X} \tag{56}$$

We initially assume that the state inequality constrains are inactive, i.e., $\eta = 0$. Therefore, with $\frac{dF_{s,\Pi}}{dt} = \mathbf{J}[F_{s,\Pi}]F$ and $\frac{dK_{s,\Pi}}{dt} = \frac{\partial K_{s,\Pi}}{\partial X} F$, the co-state dynamics are defined by:

$$\bar{\mathcal{L}} + \lambda^T \bar{F} + \gamma_b \lambda^T F_{s,\gamma} = 0 \tag{57}$$

$$\mathcal{L}_{s,\Pi} + \lambda^T F_{s,\Pi} = 0 \tag{58}$$

$$\lambda^T \mathcal{B} + \frac{\partial \mathcal{L}_{s,\Pi}}{\partial X}\big(\bar{F} + \gamma_b F_{s,\gamma}\big) - \frac{\partial \bar{\mathcal{L}}}{\partial X} F_{s,\Pi} = 0 \tag{59}$$

In Eq. (59), $\mathcal{B}$ is:

$$\mathcal{B} = \mathbf{J}[F_{s,\Pi}]\big(\bar{F} + \gamma_b F_{s,\gamma}\big) - \mathbf{J}[\bar{F} + \gamma_b F_{s,\gamma}]F_{s,\Pi} = [\mathcal{B}_1, \mathcal{B}_2, \mathcal{B}_3, \mathcal{B}_4]^T \tag{60}$$

The solution of the co-state system, Eq. (57-59), for λ_h, λ_v and λ_m reads:

$$\begin{pmatrix} \lambda_h \\ \lambda_v \\ \lambda_m \end{pmatrix} = M'^{-1} R' =: G^{\Pi_s} \tag{61}$$

In Eq. (61):

$$M' = \begin{pmatrix} \bar{F}_2 + \gamma_b F_{s2,\gamma} & \bar{F}_3 + \gamma_b F_{s3,\gamma} & \bar{F}_4 + \gamma_b F_{s4,\gamma} \\ F_{s2,\Pi} & F_{s3,\Pi} & F_{s4,\Pi} \\ \mathcal{B}_2 & \mathcal{B}_3 & \mathcal{B}_4 \end{pmatrix} \tag{62}$$

and:

$$R' = \begin{pmatrix} -\bar{\mathcal{L}} - \lambda_x(\bar{F}_1 + \gamma_b F_{s1,\gamma}) \\ -\lambda_x F_{s1,\Pi} - \mathcal{L}_{s,\Pi} \\ -\lambda_x \mathcal{B}_1 + \frac{\partial \bar{\mathcal{L}}}{\partial X} F_{s,\Pi} - \frac{\partial \mathcal{L}_{s,\Pi}}{\partial X}\big(\bar{F} + \gamma_b F_{s,\gamma}\big) \end{pmatrix} \tag{63}$$

$\Pi_s(t)$ is linked to the solution of:

$$\frac{d^2 S^{\Pi}}{dt^2} = \frac{d^2\big(\mathcal{L}_{s,\Pi} + \lambda^T F_{s,\Pi}\big)}{dt^2} = 0 \tag{64}$$

In an expanded form, Eq. (64) becomes:

$$\begin{aligned} &\frac{d}{dt}\Big(\frac{\partial \mathcal{L}_{s,\Pi}}{\partial X}\Big)\big(\bar{F} + \gamma_b F_{s,\gamma}\big) + \frac{\partial \mathcal{L}_{s,\Pi}}{\partial X}\mathbf{J}[\bar{F} + \gamma_b F_{s,\gamma}]F - \frac{d}{dt}\frac{\partial \bar{\mathcal{L}}}{\partial X} F_{s,\Pi} - \frac{\partial \bar{\mathcal{L}}}{\partial X}\mathbf{J}[F_{s,\Pi}]F + \\ &\frac{d\lambda^T}{dt}\mathcal{B} + \lambda^T \frac{d\mathcal{B}}{dt} = 0 \end{aligned} \tag{65}$$

The time derivatives of $\frac{\partial \bar{\mathcal{L}}}{\partial X}$, $\frac{\partial \mathcal{L}_{s,\Pi}}{\partial X}$ and $\mathcal{B}$ are:

$$
\begin{aligned}
&\frac{d}{dt}\frac{\partial \bar{\mathcal{L}}}{\partial X} = F^T\mathbf{J}[(\frac{\partial \bar{\mathcal{L}}}{\partial X})^T]^T = F^T\mathbf{J}[(\frac{\partial \bar{\mathcal{L}}}{\partial X})^T] \\
&\frac{d}{dt}\frac{\partial \mathcal{L}_{s,\Pi}}{\partial X} = F^T\mathbf{J}[(\frac{\partial \mathcal{L}_{s,\Pi}}{\partial X})^T]^T = F^T\mathbf{J}[(\frac{\partial \mathcal{L}_{s,\Pi}}{\partial X})^T] \\
&\frac{d\mathcal{B}}{dt} = \mathbf{J}[\mathcal{B}]F
\end{aligned} \tag{66}
$$

Eq. (65), together with Eq. (56) and Eq. (66), gives:

$$
\Pi_s(t) = \frac{\lambda^T\Big(\mathbf{J}[\bar{F}+\gamma_b F_{s,\gamma}]\mathcal{B} - \mathbf{J}[\mathcal{B}](\bar{F}+\gamma_b F_{s,\gamma})\Big) + T_1'}{\lambda^T\Big(\mathbf{J}[\mathcal{B}]F_{s,\Pi} - \mathbf{J}[F_{s,\Pi}]\mathcal{B}\Big) + T_2'} := P^{\Pi_s} \tag{67}
$$

In Eq. (67), T_1' and T_2' are:

$$
\begin{aligned}
&T_1' = -\big(\bar{F}+\gamma_b F_{s,\gamma}\big)^T\mathbf{J}[(\frac{\partial \mathcal{L}_{s,\Pi}}{\partial X})^T]\big(\bar{F}+\gamma_b F_{s,\gamma}\big) - \frac{\partial \mathcal{L}_{s,\Pi}}{\partial X}\mathbf{J}[\bar{F}+\gamma_b F_{s,\gamma}]\big(\bar{F}+\gamma_b F_{s,\gamma}\big) + \\
&\big(\bar{F}+\gamma_b F_{s,\gamma}\big)^T\mathbf{J}[(\frac{\partial \bar{\mathcal{L}}}{\partial X})^T]F_{s,\Pi} + \frac{\partial \bar{\mathcal{L}}}{\partial X}\mathbf{J}[F_{s,\Pi}]\big(\bar{F}+\gamma_b F_{s,\gamma}\big) + \frac{\partial \bar{\mathcal{L}}}{\partial X}\mathcal{B}
\end{aligned} \tag{68}
$$

$$
\begin{aligned}
&T_2' = F_{s,\Pi}^T\mathbf{J}[(\frac{\partial \mathcal{L}_{s,\Pi}}{\partial X})^T]\big(\bar{F}+\gamma_b F_{s,\gamma}\big) + \frac{\partial \mathcal{L}_{s,\Pi}}{\partial X}\mathbf{J}[\bar{F}+\gamma_b F_{s,\gamma}]F_{s,\Pi} - F_{s,\Pi}^T\mathbf{J}[(\frac{\partial \bar{\mathcal{L}}}{\partial X})^T]F_{s,\Pi} \\
&-\frac{\partial \bar{\mathcal{L}}}{\partial X}\mathbf{J}[F_{s,\Pi}]F_{s,\Pi} - \frac{\partial \mathcal{L}_{s,\Pi}}{\partial X}\mathcal{B}
\end{aligned} \tag{69}
$$

The generalized Clebsch (Legendre) condition requires:

$$
-\frac{\partial}{\partial \Pi}\frac{d^2 S^{\Pi}}{dt^2} = -\lambda^T\Big(\mathbf{J}[\mathcal{B}]F_{s,\Pi} - \mathbf{J}[F_{s,\Pi}]\mathcal{B}\Big) - T_2' \geq 0 \tag{70}
$$

In the case that the state inequality constraints are active, i.e., $\eta \neq 0$, it can be assumed an interval, $[t_c', t_d'] \subseteq [t_a', t_b']$ such that at least on element of $\mathcal{S}$ is zero; i.e., $\mathcal{S}_a = 0$. Therefore, for $t \in [t_c', t_d']$, from $\frac{d\mathcal{S}_a}{dt} = 0$,

$$
\Pi_{s,a}(t) = -\frac{\big(\frac{\partial \mathcal{S}_a}{\partial X}\big)\big(\bar{F}+\gamma_b F_{s,\gamma}\big)}{\big(\frac{\partial \mathcal{S}_a}{\partial X}\big)F_{s,\Pi}} := P^{\Pi_{s,a}} \tag{71}
$$

η_a is connected to the co-state dynamics through:

$$
\eta_a = \frac{\lambda^T\mathcal{B} + \frac{\partial \mathcal{L}_{s,\Pi}}{\partial X}\big(\bar{F}+\gamma_b F_{s,\gamma}\big) - \frac{\partial \bar{\mathcal{L}}}{\partial X}F_{s,\Pi}}{\frac{\partial \mathcal{S}_a}{\partial X}F_{s,\Pi}} \tag{72}
$$

3.3 Jump Conditions and the Complementary Theorems

The co-state variables may be discontinous at any time τ in the boundary arc interval [25]. Therefore, the jump conditions for any contact time τ read,

$$
\lambda^T(\tau^-) = \lambda^T(\tau^+) - \nu^T(\tau)\frac{\partial \mathcal{S}}{\partial X}, \quad \nu(\tau) \geq 0, \quad \nu^T(\tau)\mathcal{S} = 0 \tag{73}
$$

Since $\mathcal{S} = \mathcal{S}(h, v)$, for the active element of $\mathcal{S}$, i.e., $\mathcal{S}_a = 0$, Eq. (73) gives,

$$
\lambda_h(\tau^-) = \lambda_h(\tau^+) - \nu(\tau)\frac{\partial \mathcal{S}_a}{\partial h} \tag{74}
$$

$$\lambda_v(\tau^-) = \lambda_v(\tau^+) - \nu(\tau)\frac{\partial \mathcal{S}_a}{\partial v} \tag{75}$$

$$\lambda_x(\tau^-) = \lambda_x(\tau^+) \tag{76}$$

$$\lambda_m(\tau^-) = \lambda_m(\tau^+) \tag{77}$$

Theorem 2. *(Junction theorem in [26]) Let t_a be a time that the singular and nonsingular sub-arcs of an optimal control u are joined. Let q be the order of the singular arc. Suppose the strengthened GLC condition is satisfied at t_a, and assume that the control is piece-wise analytic in the neighborhood of t_a. Let $u^{(r)}$ be the lowest-order derivative of u that is discontinuous at t_a. Then $q + r$ is an odd integer.*

For the present OCP, $q = 1$. In addition, due to the bang/singular nature of the optimality, we suppose that the control vector itself is discontinuous, i.e., $r = 0$ for singular arc + nonsingular arc interaction. Therefore, $q + r = 1$, is an odd integer.

Theorem 3. *(theorem 5.1 in [27]) Let t_b be a time that an interior non-singular arc and a boundary arc of an optimal control u are joined. Let $u^{(r)}$ be the lowest-order derivative of u, that is discontinuous at t_b, and let p be the order of the state inequality constraints. By the assumption of $p \leq 2q + r$, if $\nu(t_b) > 0$, then $p + r$ is an even integer.*

Theorem 4. *(theorem 5.4 in [27]) Let t_c be a time that an interior singular arc and a boundary arc of an optimal control u are joined. Suppose that the strengthened GLC condition holds. Let $u^{(r)}$, be the lowest order derivative of u, that is discontinuous at t_c. By the assumption of $p \leq 2q + r$, $\nu(t_c) = 0$ and $q + r$ is an odd integer.*

For the present OCP, $p = 1$; hence, $p \leq 2q + r$ is always satisfied. The boundary arc remains in the interior of the admissible control set and in a bang/singular optimality, it can be figured as a part of the singular arc switching between $[\gamma_s, \Pi_s]^T$ and $[\gamma_{s,a}, \Pi_{s,a}]^T$. Therefore, it is reasonable to assume that the control vector itself is discontinuous in the nonsingular arc+boundary arc and singular arc+boundary arc interactions; so, $r = 0$. From theorem 3, since $p + r = 1$ is an odd integer, so $\nu(t_b) = 0$. Theorem 4 is automatically satisfied and so, $\nu(t_c) = 0$. Therefore, we can conclude that the co-state variables are continuous along the optimal trajectory.

3.4 Simplified Cases of the Closed-Form Solution

For some special cases, it is possible to extract the singular arc expressions from the closed-form solution. Through theorem 5, 6 and 7, we show that the singular arc formulas are linked to $\det[M] = 0$ or $\det[M'] = 0$ (see Appendix A).

Extraction of the singular arc formula is of help to predict the instants of the junction points in a presumed optimal structure. However, as shown in Appendix A, it is doable only for some special cases. Therefore, in principle, the presented closed-form solution still lacks identification of the number of the junction points and the corresponding instants, pending for a closing theory in optimal control. Loosely speaking, a shooting procedure is typical of this situation. In general, the singular control can be assumed as, $U_s = P(X, \lambda^T)$. However, for some cases, this form is reduced to $U_s = P(X)$. The reduced form, i.e., $U_s = P(X)$, leads to a considerable simplification in devising a solution algorithm. It is worth mentioning that the previous cited works on analytical aircraft trajectory optimization in a vertical plane fall within the category of the singular arc formula or $U_s = P(X)$.

In the following section (Sec.4), we consider the case of $U_s = P(X, \lambda^T)$ which is new and more general, and also it includes the case study that we have solved in the present work.

4 Solution Approach for $\mathcal{P}^{(2)}$

A multiple shooting procedure for the present OCP can be figured as:

$$\begin{aligned} &\Theta(Y) := [\Theta_1, ..., \Theta_{N+1}]^T, \quad \Theta \in \mathbb{R}^{N+1} \\ &Y = [\tilde{t}_1, ..., \tilde{t}_N, \lambda_x(t^*)]^T, \quad \tilde{t}_N = t_f \quad Y \in \mathbb{R}^{N+1} \end{aligned} \tag{78}$$

In Eq. (78), $\Theta_k, k = 1, ..., N+1$ are the boundary (closing) equations and $\tilde{t}_k, k = 1, ..., N$ are the number of junction points. In addition, t^* is a junction point joining a bang extremal to a singular extremal.

In a conventional manner, the closing equations are,

$$\begin{aligned} &\Theta_{1:q\leq 4} = \phi_f(X_f) = X_f - X(t_f) = 0 \\ &\Theta_{q+1} = \mathcal{H}(t_f) = 0 \end{aligned} \tag{79}$$

In the case that $q \neq 4$, we can consider $\lambda_4(t_f) = ... = \lambda_{q+1}(t_f) = 0$. Therefore, normally, $\Theta \in \mathbb{R}^5$. This means that a standard shooting procedure can handle a limited number of the shooting parameters, i.e., $Y \in \mathbb{R}^5$. However, there may exist cases with additional shooting parameters, e.g., an optimal solution with BSB structure for both $\gamma(t)$ and $\Pi(t)$.

Therefore, in general, in order to automate the solution procedure (to extricate it from searching for amenable closing equations), we propose an alternative solution approach; that is to translate the shooting problem into a very sparse parameter optimization in the following form:

$$\begin{aligned} &\min_{\lambda_x(t^*),\tilde{t}_k,k=1,...,K\in\mathbb{N}} \mathcal{J} = \Phi(X(\tilde{t}_K), \tilde{t}_K) \\ &s.t. \\ &\frac{dX}{dt} = F(X, \lambda_x(t^*)) \\ &\phi_0(X(t_0), t_0) = 0 \\ &\phi_f(X(\tilde{t}_K), \tilde{t}_K) = 0 \end{aligned} \tag{80}$$

First, we interpret the representation of the junction points in a parameter optimization. Next, for a minimum time problem, we compare the shooting results with those from a corresponding parameter optimization and draw the conclusion that, conversion of the shooting problem to a very sparse parameter optimization surpasses in terms of labor, automation and also insertion of the boundary conditions for $\gamma(t)$ with an analogous level of accuracy and computational time (see Appendix A).

4.1 The Proposed Algorithm for $\mathcal{P}^{(2)}$

With the help of theorem 1, we design an algorithm (see Algorithm 1) that the unknown parameters are only the junction points, $\tilde{t}_k$ and $\lambda_x(t^*)$. Algorithm 1 allows the possible switches inside and outside the singular extremals. The maximum number of singular extremals are assumed to be one for $\gamma(t)$ and one for $\Pi(t)$. Algorithm 1 (in its current form) is applicable to the simulation of a mixed climb/cruise phase. However, with slight modifications, the logic is extendable to the case of mixed cruise/descent phase and free routing flights.

With λ^T known over the entire time domain, it is straightforward to verify the optimality of the singular extremals by computing Eq. (51) and Eq. (70). In addition, the switching functions can be computed to check the first order optimality condition of the bang extremals. Initializing the bang extremals for $\gamma_{b2:b5}$ and $\Pi_{b1:b4}$ seems to be a try and error procedure and in most cases, we verified that $\gamma_{b2} = ... = \gamma_{b5}$ and $\Pi_{b1} = ... = \Pi_{b4}$. However, in practice, we were able to obtain the optimal solutions by initiating the algorithm with different combinations of the extremals. In this situation, we sometimes witnessed some pulses in the optimal solutions which were linked to the wrong extremals. More specifically, suppose that the preset γ_{bi} over $(\tilde{t}_{i+1} : \tilde{t}_{i+2})$ is not optimal. In this case, the optimization module computes $(\tilde{t}_{i+1} \approx \tilde{t}_{i+2})$ secured to some decimal places. This very marginal deviation shows itself as a pulse. Nonetheless, a verified structure preserves itself in a range of variations over the relaxed parameters involved.

5 Case Study

In this section, we set the objective functional as to be a combination of the arrival time and fuel burn and solve the OCP for a partial climb phase. In the following, we explore the appearance of

Algorithm 1 The Multi-Structure Detection Algorithm

Figuring the extremals as:
$(0, \tilde{t}_1) : \gamma_{b1}, \Pi_{b1}$
$(\tilde{t}_1, \tilde{t}_2) : \gamma_s, \Pi_{b2}$
$(\tilde{t}_2, \tilde{t}_3) : \gamma_s, \Pi_{b3}$
$(\tilde{t}_3, \tilde{t}_4) : \gamma_{b2}, \Pi_{b4}$
$(\tilde{t}_4, \tilde{t}_5) : \gamma_{b3}, \Pi_s$
$(\tilde{t}_5, \tilde{t}_6) : \gamma_{b4}, \Pi_s$
$(\tilde{t}_6, \tilde{t}_7 := t_f) : \gamma_{b5}, \Pi_{b5}$
The decision variables are: $\tilde{t}_k : k = 1 : 7, \lambda_x(\tilde{t}_1)$.
Assumption:
$\gamma_{s,a} \subseteq \gamma_s$
$\Pi_{s,a} \subseteq \Pi_s$
Initializing the bang extremals:
$\gamma_{bi}, i = 1 : 5 \leftarrow (\gamma_{min} \vee \gamma_{max})$
$\Pi_{bi}, i = 1 : 5 \leftarrow (\Pi_{min} \vee \Pi_{max})$
Initializing the decision variables:
$\tilde{t}_k := \tilde{t}_k^{(0)} k = 1 : 7, \lambda_x(\tilde{t}_1) := \lambda_x^{(0)}(\tilde{t}_1^{(0)})$
Integration process:
a) Solving $\frac{dX}{dt} = F(X, U)$ over $(0, \tilde{t}_1^{(0)})$
b) Solving $\frac{dX}{dt} = F(X, U)$ and $\frac{d\lambda_x}{dt} = -\frac{\partial \mathcal{H}}{\partial x}$ simultaneously over $(\tilde{t}_1^{(0)}, \tilde{t}_2^{(0)})$ with:
$\lambda_h, \lambda_v, \lambda_m := G(X, \lambda_x)$
$\gamma_s := P^{(\gamma)}(X, \lambda)$
c) Solving $\frac{dX}{dt} = F(X, U)$ by forward integration from $\tilde{t}_2^{(0)}$ to $\tilde{t}_f^{(0)}$and $\frac{d\lambda^T}{dt} = -\frac{\partial \mathcal{H}}{\partial X}$ by backward and forward integration from $\tilde{t}_1^{(0)}$ to $\tilde{t}_0^{(0)} =: 0$ and $\tilde{t}_2^{(0)}$ to $\tilde{t}_f^{(0)}$ with:
$\Pi_s := P^{(\Pi)}(X, \lambda)$
Solving the associated NLP

the various scenarios captured by Algorithm 1. More specifically, by changing α from 1 to 0, the OCP alters from the pure minimum time to the pure minimum fuel. For the simulated range of the parameters involved, $\alpha = 1$ corresponds to a uniform B structure for $\Pi(t)$, i.e., $\Pi^*(t) = \Pi_{max}$. However, the optimal structure for $\gamma(t)$ includes one singular extremal. It is noteworthy mentioning that $\alpha = 1$ corresponds to the case of one active singular control (as mentioned before, the case of one active singular control has been the target of numerous previous works). As α changes from 1 to 0, the optimal $\Pi(t)$ can be BB or BSB; whilst, the optimal $\gamma(t)$ is mostly BSB.

For the comparison purpose, the optimal solutions due to PMP are labeled as the *analytical solutions* and those from the direct approach are labeled as the *numerical solutions*.

5.1 Problem Setup

In order to engage the full dynamics, we simulate a partial climb phase. The objective is considered as a combination of the flight time and the fuel burn:

$$\mathcal{L} = \alpha + (1 - \alpha)\Pi C_s T, \quad \alpha \leq 0 \leq 1 \tag{81}$$

T, C_s and D are simulated by Base of Aircraft DAta (BADA) model from EUROCONTROL providing a general smooth aircraft performance model [28]. In addition, air density is approxi-

mated by International Standard Atmospheric (ISA) model:

$$
\begin{aligned}
&T(h) = C_{T_1}\big(1 - \frac{h}{C_{T_2}} + h^2 C_{T_3}\big), \quad C_s(v) = C_{s_1}\big(1 + \frac{v}{C_{s_2}}\big) \\
&P(h) = P_0\big(\frac{\Theta(h)}{\Theta_0}\big)^{\frac{g}{\beta R}}, \quad \Theta(h) = \Theta_0 - \beta h, \quad \rho(h) = \frac{P(h)}{R\Theta(h)} \\
&D(m, v, h) = \frac{1}{2}\rho(h) s v^2 \big(C_{D_1} + C_{D_2} C_l^2\big)
\end{aligned}
\tag{82}
$$

Where, s is the aerodynamic lift surface and ρ is the air density. $C_{T_i}, i = 1, 2, 3$, s, $C_{D_i}, i = 1, 2$, $C_{s_i}, i = 1, 2$, R, β, P_0 and θ_0 are known constants.

The model constants as well as the fixed boundaries for different scenarios are tabulated for a medium-haul aircraft (see Table 1).

Table 1: The model constants and the fixed boundary conditions

Parameter	Value	Unit (SI)	Parameter	Value	Unit (SI)
$h(0)$	3480	m	$v(0)$	151.67	m/s
$h(t_f)$	9144	m	$v(t_f)$	191	m/s
s	122.6	m^2	g	9.81	m/s^2
C_{T_1}	141040	N	C_{T_2}	14909.9	m
C_{T_3}	$6.997e^{-10}$	m^{-2}	C_{D_1}	0.0242	–
C_{D_2}	0.0469	–	C_{s_1}	$1.055e^{-5}$	$kg.s^{-1}N^{-1}$
C_{s_2}	441.54	$m.s^{-1}$	R	287.058	$J.kg^{-1}K^{-1}$
Θ_0	288.15	K	β	0.0065	$K.m^{-1}$
P_0	101325	Pa	$x(0)$	0	m
M_{cr}	0.8	–	$m(t_f)$	$relaxed$	kg

We consider a rather arbitrary wind field as:

$$
w(x, h) = a_w^0\big(a_w^1 h^2 - a_w^2 \times 10^{-8} x^2 + 10^{-4} x\big) \tag{83}
$$

The adjustable parameters a_w^0, a_w^1 and a_w^2 can produce different wind profiles ranging from smooth to severe pure positive (or pure negative) winds as well as mixed positive/negative winds of smooth or severe types. The latter case is to naively imitate the presence of storms. Some of the distinct profiles simulated in this work are graphed (see Fig. 2).

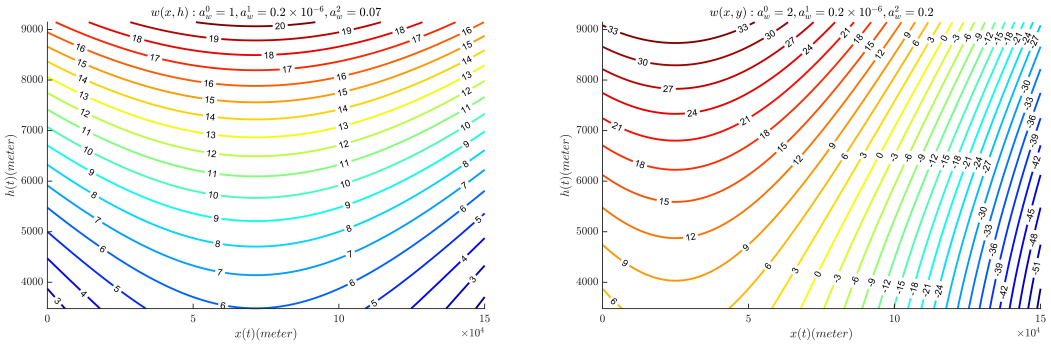

(a) (b)

Figure 2: a view on two different wind profiles duo to Eq. (83)

5.2 Results

The results of the present simulation are given through subsec.5.2.2-5.2.5. The direct numerical solution procedure for $\mathcal{P}^{(1)}$ is specified in subsec.5.2.1.

5.2.1 Numerical Solution for $\mathcal{P}^{(1)}$

For the numerical solution, we solve the complete model (sec.2) based on Adams-Bashforth [29] discrete scheme of the second order with a piece-wise constant assumption for the control vector, $U = [C_l(t), \Pi(t)]^T$. The resulting NLP can be figured as:

$$\begin{aligned}
&\min_{t_N, C_l(t_i), \Pi(t_i), i=1,\dots,N} \mathcal{J} = \alpha t_N + (1-\alpha)\big(X_4(t_0) - X_4(t_N)\big) \\
&s.t. \\
&\frac{dX}{dt} = F(X, C_l, \Pi), \quad X, F \in \mathbb{R}^5 \\
&\Phi_0\big(X(t_0)\big) = 0, \quad \Phi_0 \in \mathbb{R}^5 \\
&\Phi_N\big(X(t_N)\big) = 0, \quad \Phi_N \in \mathbb{R}^4 \\
&0 \le X_5 \le X_{5,max}, \quad \Pi_{min} \le \Pi \le 1 \\
&G(X) \le 0, \quad G \in \mathbb{R}^2
\end{aligned} \tag{84}$$

Where, $X = [x, h, v, m, \gamma]^T$. In order to simulate the partial climb phase, the boundary conditions for X_5 are considered as:

$$X_5(t_0) = X_5(t_N) = 0 \tag{85}$$

For the numerical solution, interior-point/barrier algorithm of the NLP solver fmincon from MATLAB® Optimization Toolbox, was adopted as the optimization module.

5.2.2 Scenario 1: $\overbrace{BSB}^{\gamma(t)}+\overbrace{B}^{\Pi(t)}$

In this subsection, we explore $BSB+B$ structure that is the case with one active singular control. We consider the case with $\alpha = 1$ corresponding to the minimum time problem. For the simulated range of the parameters involved, the optimal solution for $\Pi(t)$ was confirmed to be a uniform bang structure; i.e., $\Pi^*(t) = \Pi_b = \Pi_{max} = 1$. For the case of $NoWind$ ($a_w^0 = 0$) with $m(0) = 69000$, $\gamma_{min} = 0$, $\gamma_{max} = 0.2$ and varying $x(t_f)$, the analytical solutions for $\gamma(t)$ and the state variables are compared with the numerical ones in Fig. 3. From these plots, it becomes clear that the singular and the boundary extremals are perfectly covered.

Fig. (4) shows a comparison for $\gamma(t)$ between the analytical solutions and the numerical ones for two distinct cases with wind consideration.

A better comparison is to compare the optimal objective and the final mass. In this respect, these differences between the analytical and numerical solutions are tabulated (see table 2). The differences are defined as, $|\Delta t_f| = |t_f^{analytical} - t_f^{numerical}|$, $|\Delta m_f| = |m_f^{analytical} - m_f^{numerical}|$. Interestingly, the deviation is negligible.

5.2.3 Scenario 2: $\overbrace{BSBB, aBB}^{\gamma(t)}+\overbrace{B}^{\Pi(t)}$

In this scenario, $\alpha = 1$ and for the simulated range of parameters, $\Pi^*(t)$ was confirmed to be a uniform bang structure; i.e., $\Pi^*(t) = \Pi_b = 1$. The BSBB structure may exist for a range of the involved parameters. However, in the present simulation, BSBB for $\gamma(t)$ was captured in larger values of γ_{min} and specified m_f. As γ_{min} increases, the optimal structure for $\gamma(t)$ changes from BSB to BSBB. Thereafter, the new structure, BSBB, is dominant and the singular extremal shrinks

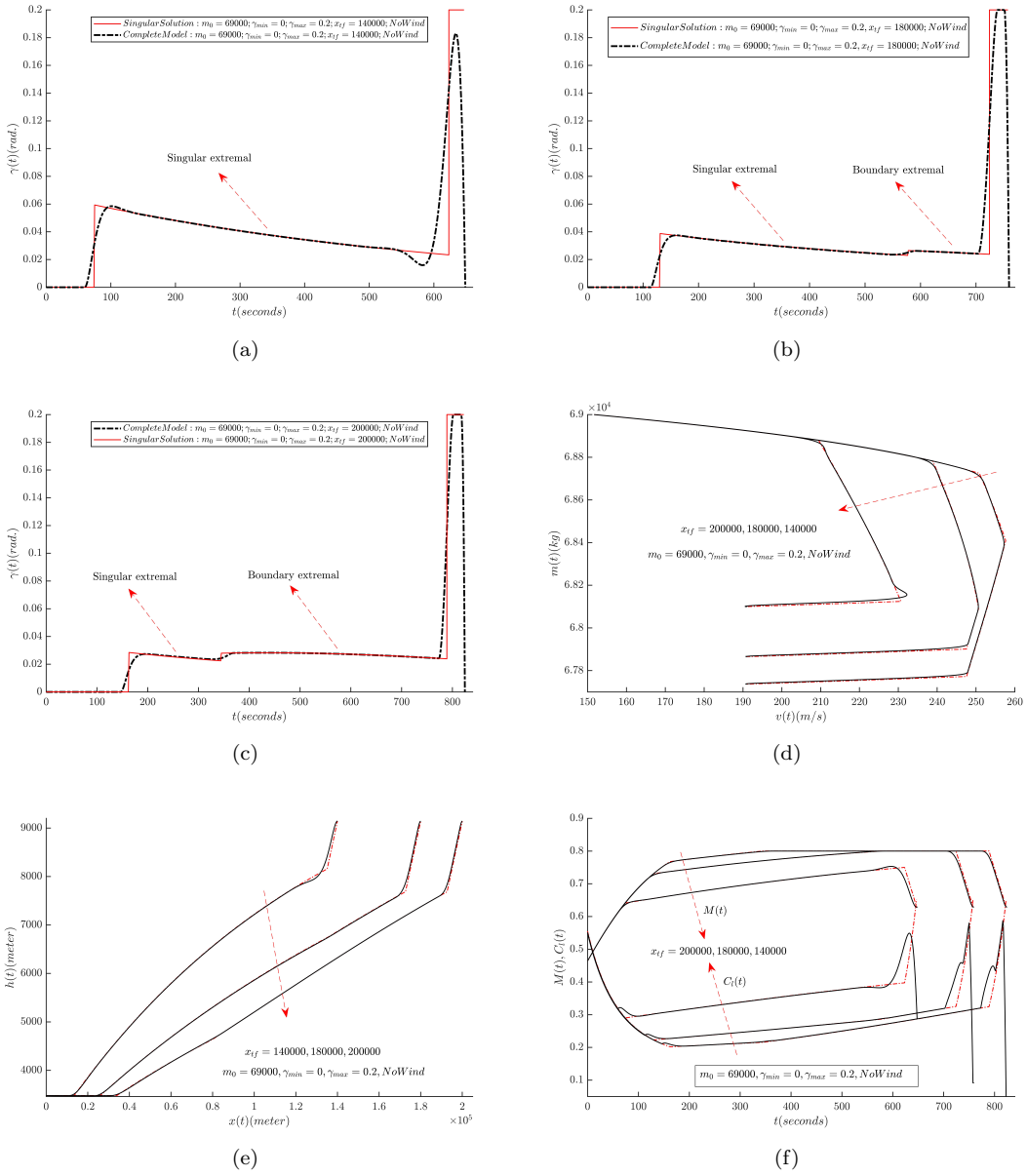

Figure 3: $\gamma(t)$ and the state variables: the impact of $x(t_f)$, $\alpha = 1$, $NoWind$ ($a_w^0 = 0$); Red Lines: Analytical Solutions, Black Lines: Numerical Solutions

Table 2: $|\Delta t_f|$ and $|\Delta m_f|$ for BSB+B structure; $m_0 = 69000, \gamma_{min} = 0, \gamma_{max} = 0.2, a_w^0 = 0$

x_f	$\lvert\Delta t_f\rvert(s)$	$\lvert\Delta m_f\rvert(kg)$
140000	1.22	0.27
160000	1.17	0.28
180000	1.31	0.34
200000	1.42	0.32
220000	1.26	0.35

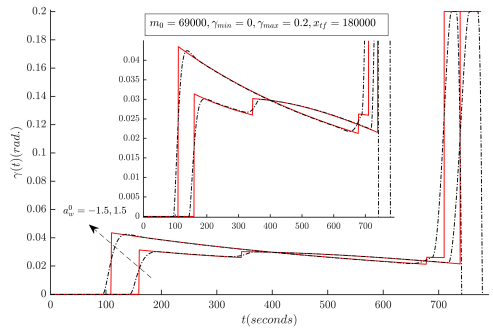

(a)

Figure 4: $\gamma(t)$: the impact of wind, $\alpha = 1$, $(a_w^1 = 0.2 \times 10^{-6}, a_w^2 = 0.07)$; Red Lines: Analytical Solutions, Black Lines: Numerical Solutions

as γ_{min} increases. This shrinkage continues until the singular extremal disappears asymptotically; turning BSBB to aBB in a critical γ_{min}, i.e., $\gamma_{min,cr.}$. Therefore, aBB is the closing optimal structure since for $\gamma_{min} > \gamma_{min,cr.}$, the number of boundary equations are more than the shooting parameters and therefore, in principle, the shooting system is inconsistent.

For the sake of brevity, we only graph the main variable, $\gamma(t)$. Fig. 5 shows a comparison between the analytical solutions and the numerical ones for fixed γ_{min} and $a_w^0 = 0$ (Fig. 5-a) and varying γ_{min} (Fig. 5-b). Fig. 6-a and Fig. 6-b display the analytical solutions for positive and negative wind profiles respectively with $\gamma_{max} = 0.15$. Fig. 6-c shows the analytical solutions indicating the evolution of BSBB to aBB for $a_w^0 = 0$. In addition, table 3 depicts $|\Delta t_f|$ for some stages with $m_0 = 69000$, $\gamma_{max} = 0.15$, $m_f = 68100$, $x_f = 140000$.

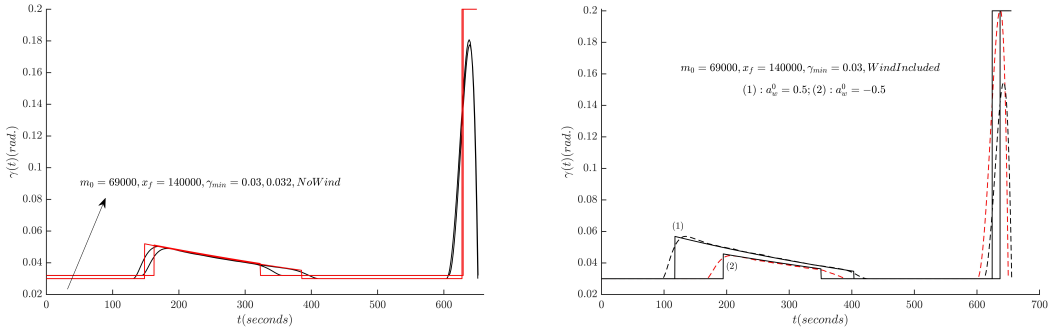

(a) (b)

Figure 5: $\gamma(t)$: BSBB comparison; Red Lines: Analytical Solutions, Black Lines: Numerical Solutions $(m_f = 68100, a_w^1 = 0.2 \times 10^{-6}, a_w^2 = 0.07)$

Table 3: $|\Delta t_f|$ BSBB+B structure; $a_w^0 = -0.5, a_w^1 = 0.2 \times 10^{-6}, a_w^2 = 0.07$

γ_{min}	$\lvert\Delta t_f\rvert(s)$
0.027	0.93
0.029	0.95
0.031	0.91
0.033	0.97

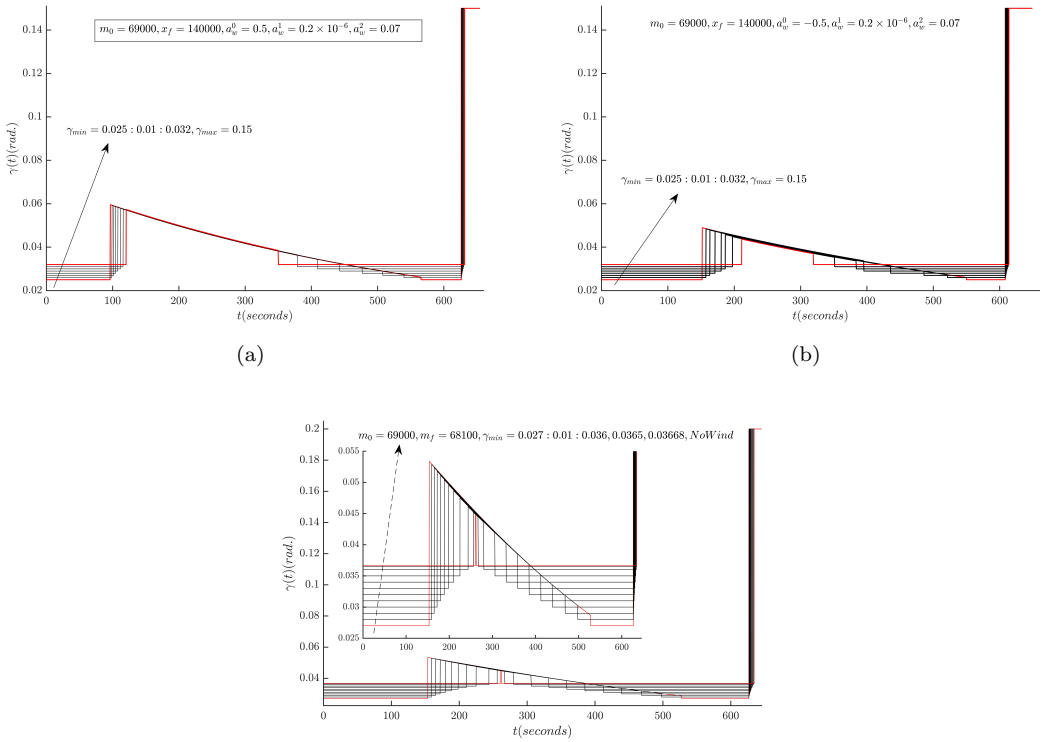

Figure 6: $\gamma(t)$: BSBB; $m_f = 68100, a_w^1 = 0.2 \times 10^{-6}, a_w^2 = 0.07$

5.2.4 Scenario 3: $\overbrace{BSB}^{\gamma(t)}+\overbrace{BB}^{\Pi(t)}$

In order for BB structure of $\Pi(t)$ to appear, the involved parameters need to change. In this respect, we set $\alpha = 0.7$ and adjust the other involved parameters to emphasize the existence of BB structure for $\Pi(t)$. For the case that the state inequality constraints are inactive, i.e., $\eta(t) = 0$, the optimal controls as well as the corresponding optimal states are graphed in Fig. 7. The effect of Π_{min} with active state inequality constraints and $a_w^0 = 0$ is shown in Fig. 8. Fig. 9 shows the impact of wind on the evolution of the optimal solutions with $\Pi_{min} = 0.9$. Fig. 10 displays a comparison between the analytical solutions and the numerical solutions for the case of $\Pi_{min} = 0.9$. Table 5 shows the results for $|\Delta t_f|$ and $|\Delta m_f|$ clarifying a remarkable resemblance between the two solution approaches.

Table 4: $|\Delta t_f|$ and $|\Delta m_f|$ for BSB+BB structure; $m_0 = 59000, x_f = 150000, \gamma_{min} = 0, \gamma_{max} = 0.15, a_w^0 = 1, a_w^1 = 0.2 \times 10^{-6}, a_w^2 = 0.07$

Π_{min}	$\lvert\Delta t_f\rvert(s)$	$\lvert\Delta m_f\rvert(kg)$
0.95	1.12	0.15
0.9	0.98	0.13
0.85	0.93	0.11
0.8	1.03	0.13

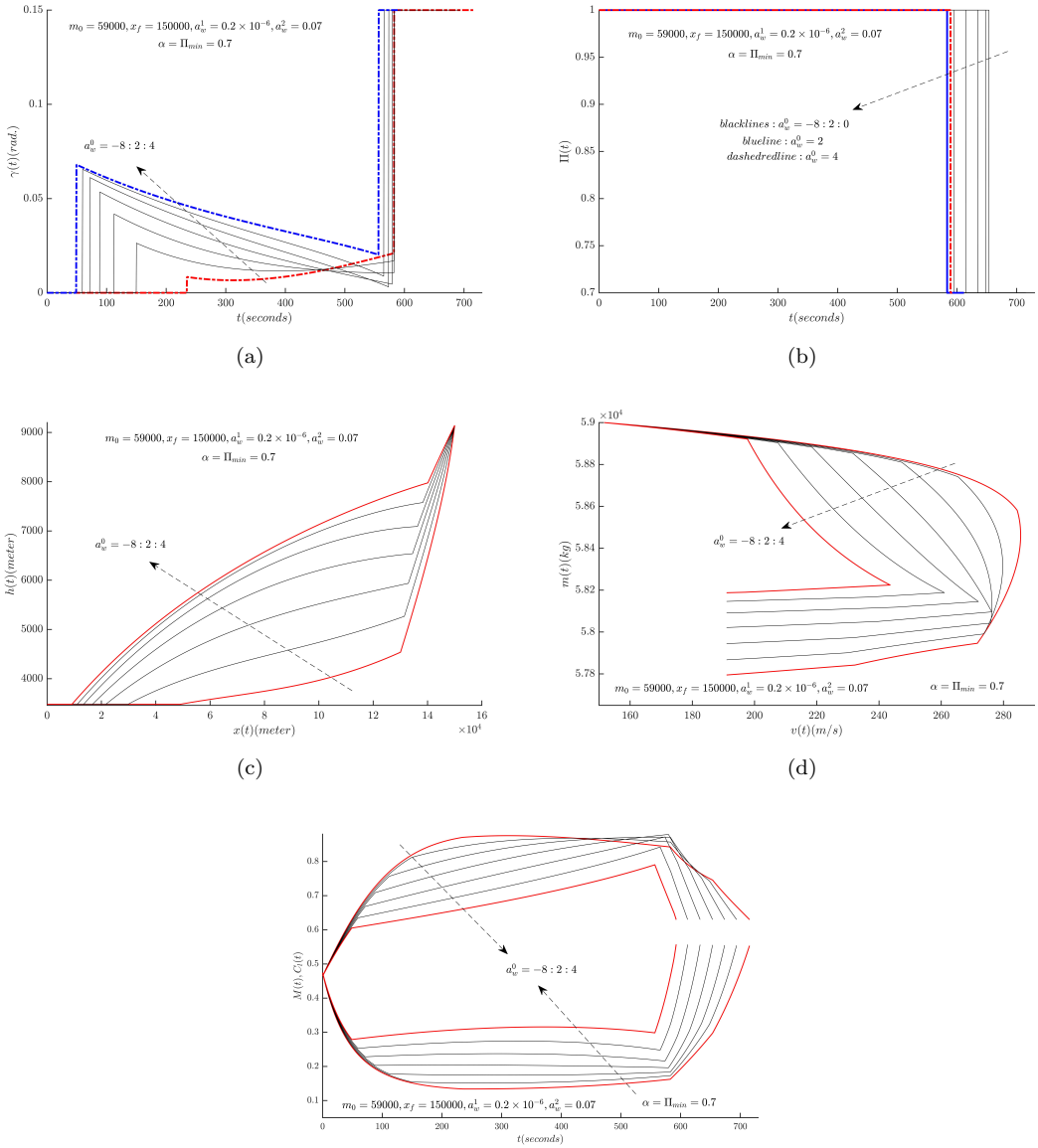

Figure 7: BSB+BB; $\eta(t) = 0$, $m_0 = 59000, \gamma_{min} = 0, \gamma_{max} = 0.15, \Pi_{min} = 0.7, x_f = 150000, a_w^1 = 0.2 \times 10^{-6}, a_w^2 = 0.07$

5.2.5 Scenario 4: $\overbrace{BSB}^{\gamma(t)}+\overbrace{BSB}^{\Pi(t)}$

In this scenario, we set $\alpha \leq 0.25$ and, in particular, examine the effects of Π_{min}, α and wind. Fig. 11 shows the impacts of Π_{min} and α in the presence of wind. From these plots, as α decreases, the singular extremal for $\Pi(t)$ expands. Fig. 12 shows the impact of a severe mixed positive/negative wind with $\Pi_{min} = 0.3$ on the evolution of BSB+BSB structure. The wind profile used in the production of Fig. 12 naively captures some of the characteristics of a storm. This, by itself, highlights the applicability of the proposed analytical approach to handle complex phenomena. In this scenario, the numerical solutions show severe chattering response due to the fact that the OCP is singular on $\Pi(t)$. We only show a comparison between the analytical solutions and

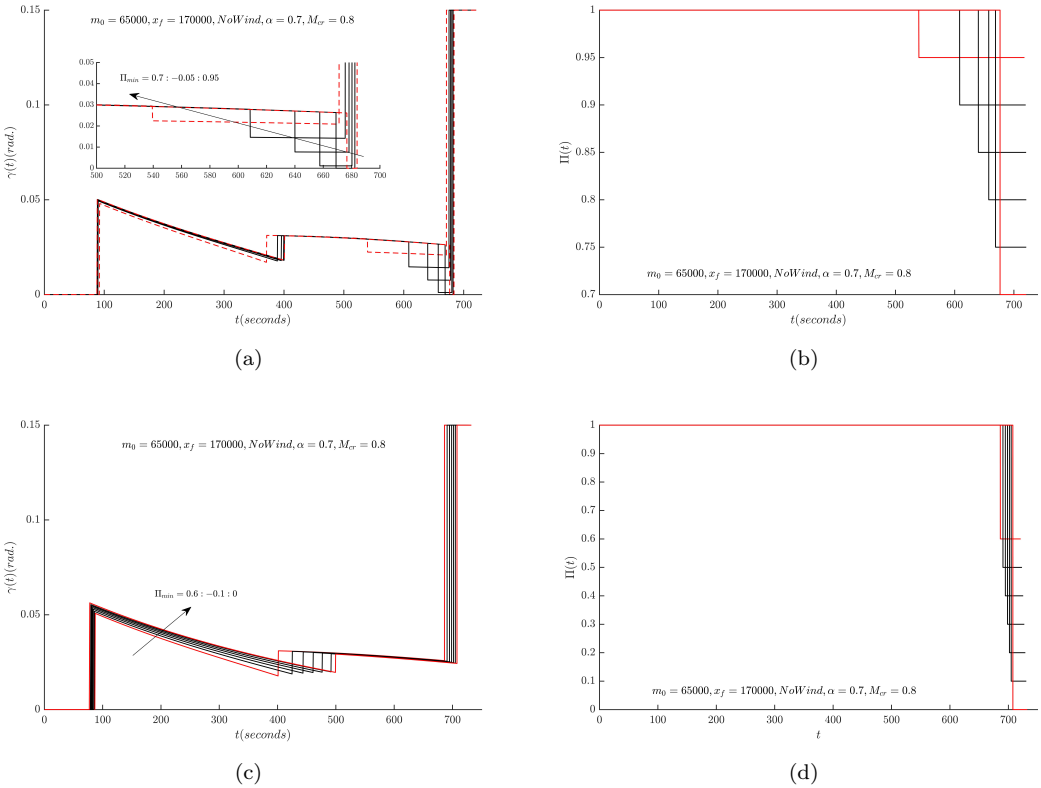

Figure 8: BSB+BB; $m_0 = 65000, \gamma_{min} = 0, \gamma_{max} = 0.15, x_f = 170000, a_w^0 = 0$: (a) and (b) belong to $\Pi_{min} : 0.95 - 0.05 : 0.7$. (c) and (d) belong to $\Pi_{min} : 0.6 - 0.1 : 0$

the numerical ones for $\gamma(t)$ and $\Pi(t)$ and this suffices to clarify the superiority of the analytical solutions (see Fig. 13). Table 5.2.5 is devoted to a comparison for $|\Delta t_f|$ and $|\Delta m_f|$. Unexpectedly, the deviation is clearer. This deviation is perhaps due to the inaccurate results from the numerical solutions.

Table 5: $|\Delta t_f|$ and $|\Delta m_f|$ for BSB+BSB structure; $m_0 = 59000, x_f = 150000, \gamma_{min} = 0, \gamma_{max} = 0.15, a_w^0 = -1, a_w^1 = 0.2 \times 10^{-6}, a_w^2 = 0.07$

α, Π_{min}	$\lvert\Delta t_f\rvert(s)$	$\lvert\Delta m_f\rvert(kg)$
0	7.68	0.86
0.1	4.32	0.67
0.25	2.53	0.45

6 Conclusion

It was presented a mathematical framework for commercial aircraft trajectory optimization in a vertical plane with two active singular controls, an arbitrary objective function, equality and inequality constraints as well as arbitrary wind profiles (Sec. 3). Conventionally, a shooting procedure is typical of this problem ($\mathcal{P}^{(2)}$). However, we translated the shooting procedure into a very sparse NLP and gave mathematical justifications for the correspondence (Sec.4). An algorithm (Algorithm 1) was proposed, able to capture multiple combinations of bang/singular extremals. Algorithm 1 is also able to capture the effects of boundary conditions for $\gamma(t)$ through a zeroth

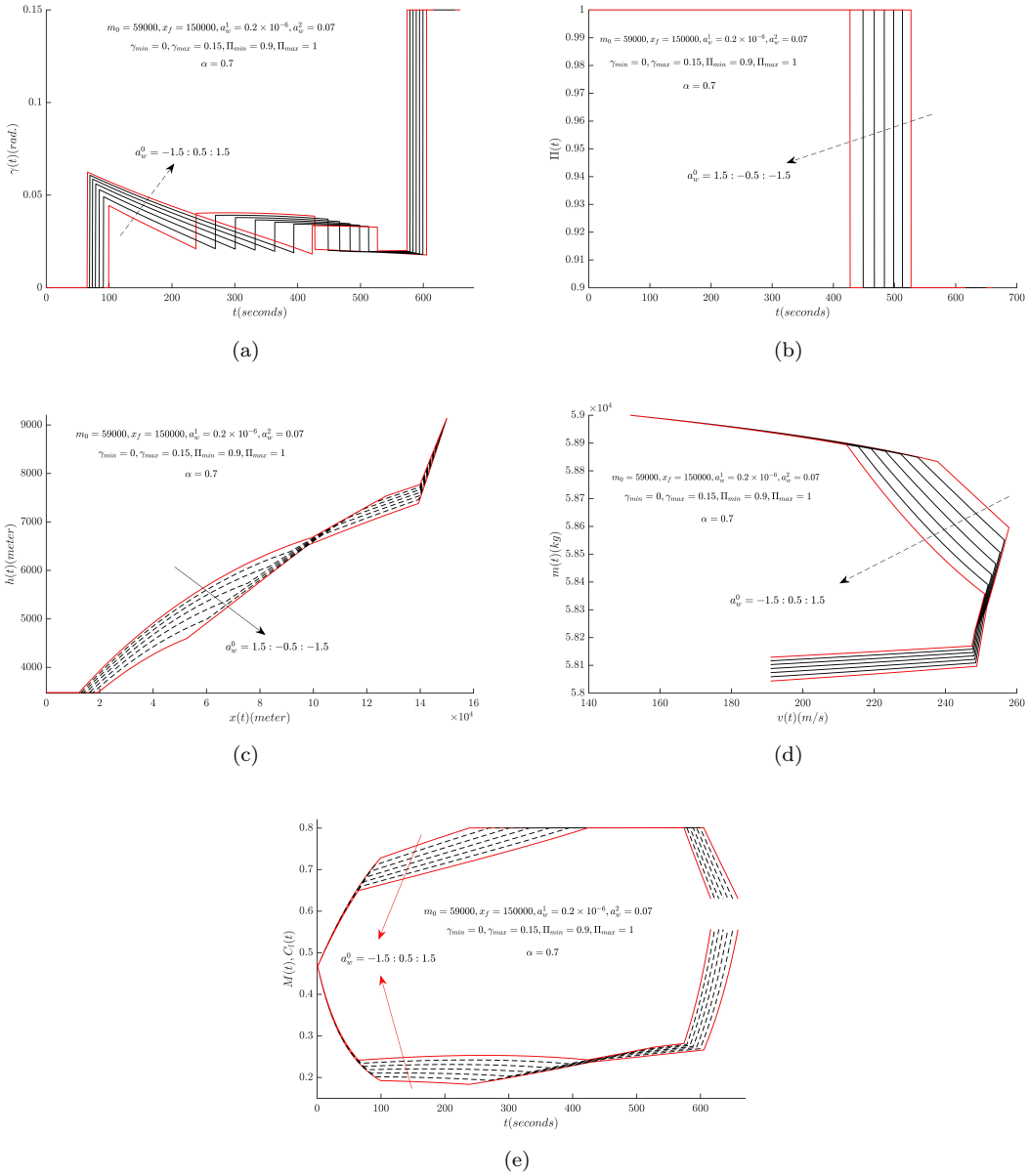

Figure 9: BSB+BB; $m_0 = 59000, \gamma_{min} = 0, \gamma_{max} = 0.15, x_f = 150000$

order expansion scheme which includes additional junction points. Specifically, we compared the optimal results due to $(\mathcal{P}^{(2)})$ with those from $(\mathcal{P}^{(1)})$ with the overall conclusion of remarkable accuracy. Through the case study, we showed in Sec. 5.2.4 that a pure climb phase (not ending up with a cruise phase) may involve optimal $\Pi(t)$ in the form of BB with switching instants inside or outside the singular $\gamma(t)$. More specifically, this new structure can be understood through the objective function which was a combination of the arrival time and the fuel burn. In addition, we showed in Sec. 5.2.3 the existence of optimal structures for $\gamma(t)$ other that BSB, i.e., BSBB and aBB which were also new in view of the analytical aircraft trajectory optimization.

It is well-known that the optimal solutions by PMP involve some complications especially in complex problems and inherently, PMP approach to OCP is more difficult, in terms of labor and implementation, than a direct NLP approach. A good deal of this difficulty is addressed to the initialization of the multipliers (whether to be the state equality multipliers, co-states, or

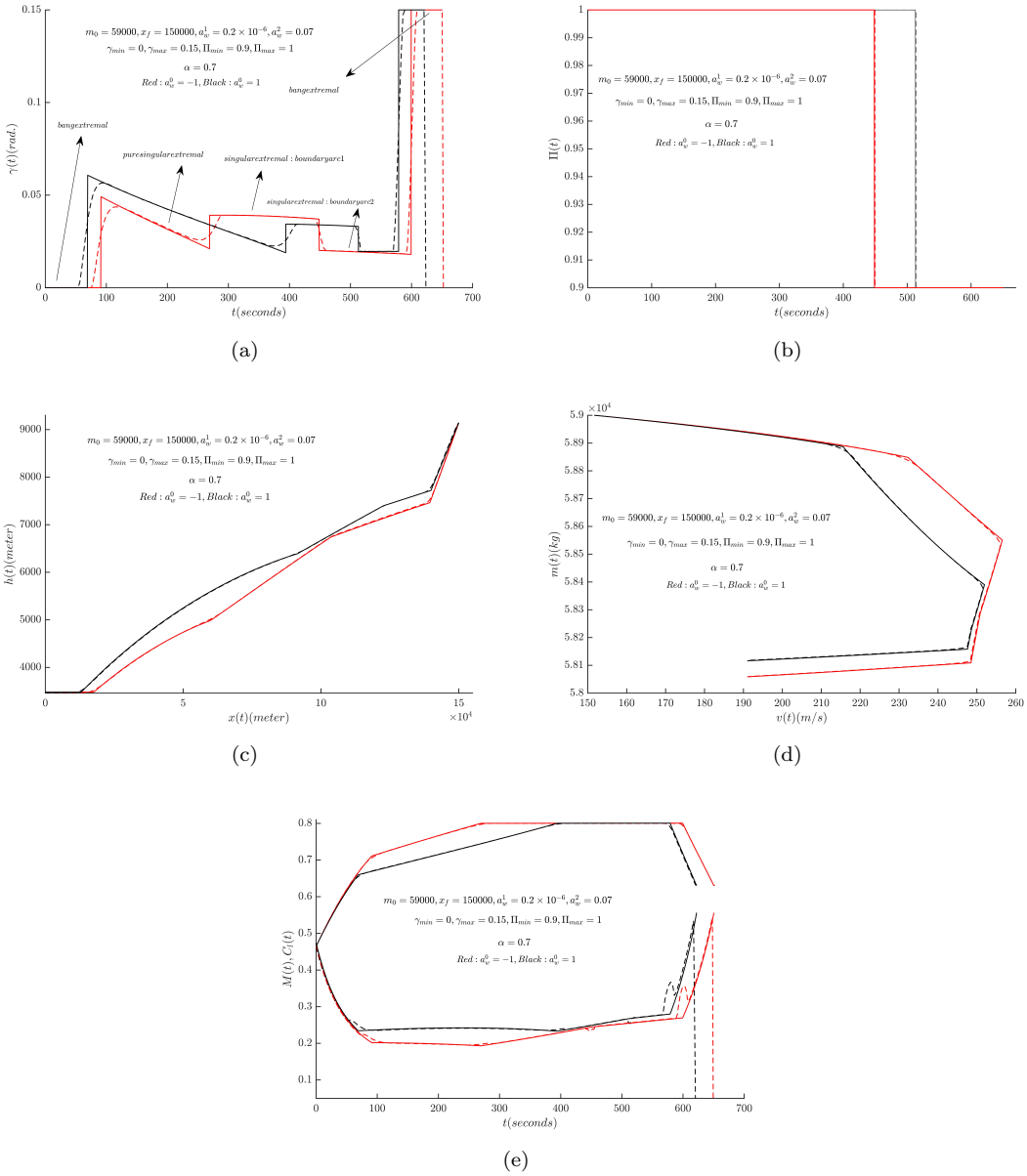

Figure 10: BSB+BB; $m_0 = 59000, \gamma_{min} = 0, \gamma_{max} = 0.15, x_f = 150000$

those from the inequality constraints). Nevertheless, for a singular OCP, the PMP approach may lead to a considerable simplification. On the other hand, in a direct optimization, the projected Hessian matrices are ill-posed if the problem is singular. Hence, concerning the accuracy and the computational time for a singular OCP, the PMP approach prevails.

The presented closed-form solution for $\mathcal{P}^{(2)}$ was verified to be quite efficient and accurate especially when the optimal structure is identified. The notable point is that an identified structure likely preserves itself over a range of the relaxed parameters. It is hopeful that the present work is evident enough that the singular PMP approach is applicable to more complex arenas regarding the commercial aircraft trajectory optimization.

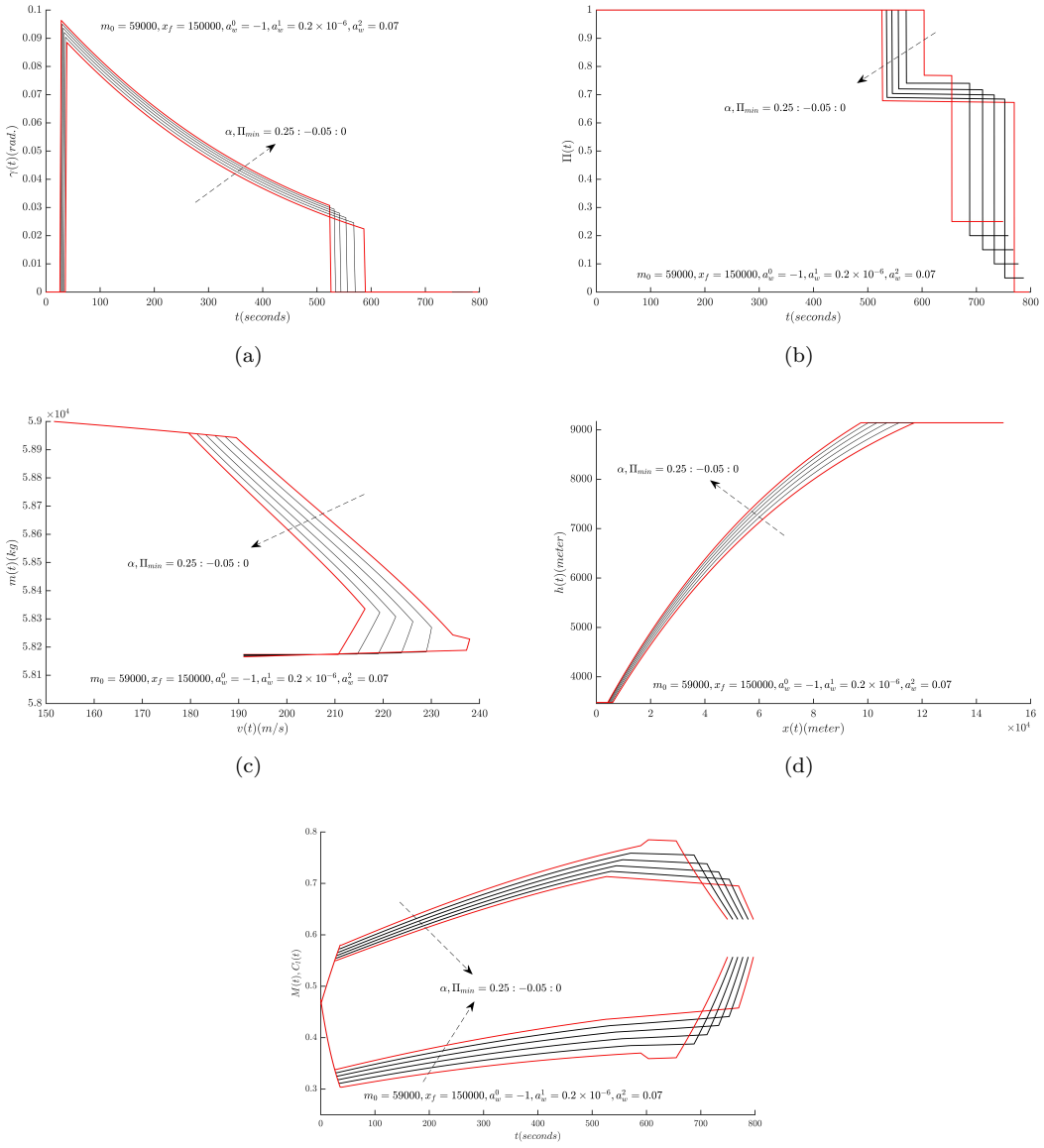

Figure 11: BSB+BSB: the effects of Π_{min} and α: $m_0 = 59000, \gamma_{min} = 0, \gamma_{max} = 0.15, x_f = 150000$

A Appendix A

Theorem 5. *If $\lambda_x(t) = 0$, the singular arc of $\gamma(t)$, is defined by* $\det[M] = 0$ *and the occurrence is subject to $\mathcal{L} = c(x, m)\hat{F}_4$ ($\hat{F} := \bar{F} + \Pi F_{s,\Pi}$).*

Proof. For the singular arc to be defined purely in terms of the state variables, we rewrite the algebraic equations (Eq. (37),(38), (39)), taking into account, $\lambda_x(t) = 0$ and $F_{s1,\gamma} = F_{s4,\gamma} = \hat{F}_2 = 0$, as:

$$\det[M] \begin{pmatrix} \lambda_h \\ \lambda_v \\ \lambda_m \end{pmatrix} = \begin{pmatrix} \mathcal{A}_4 F_{s3,\gamma} & \mathcal{A}_3\hat{F}_4 - \mathcal{A}_4\hat{F}_3 & -\hat{F}_4 F_{s3,\gamma} \\ -\mathcal{A}_4 F_{s2,\gamma} & -\mathcal{A}_2\hat{F}_4 & \hat{F}_4 F_{s2,\gamma} \\ \mathcal{A}_3 F_{s2,\gamma} - \mathcal{A}_2 F_{s3,\gamma} & \mathcal{A}_2\hat{F}_3 & -\hat{F}_3 F_{s2,\gamma} \end{pmatrix} \begin{pmatrix} -\mathcal{L} \\ 0 \\ \left(\frac{\partial \mathcal{L}}{\partial X}\right) F_{s,\gamma} \end{pmatrix} \tag{86}$$

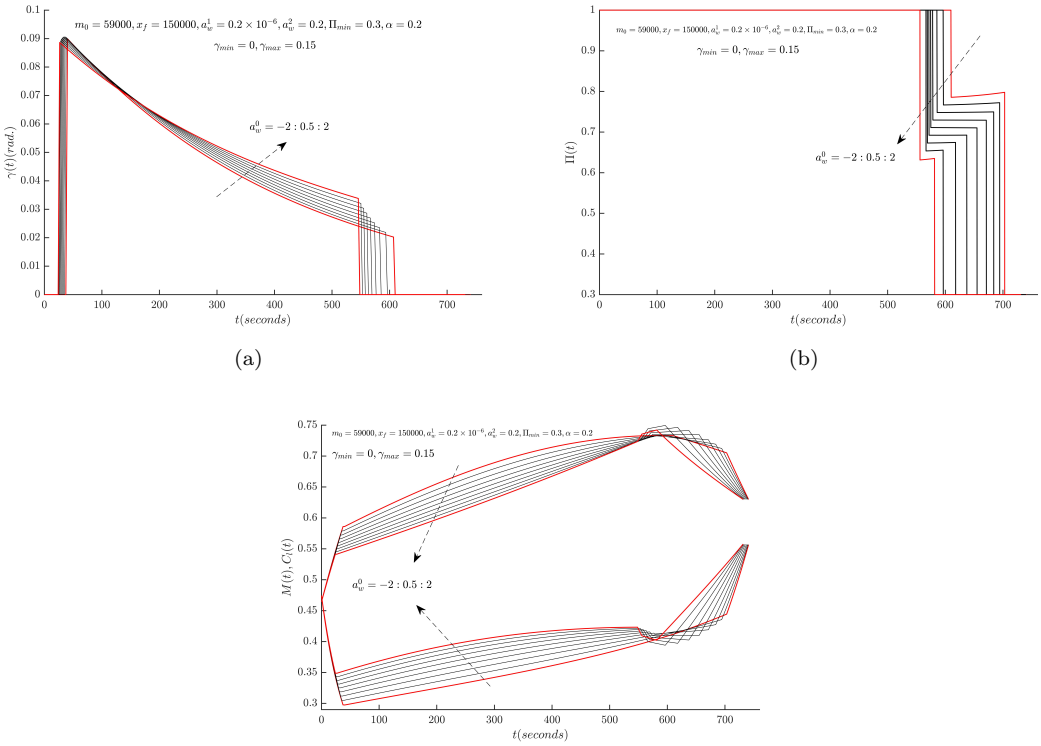

(a) (b)

(c)

Figure 12: BSB+BSB: the effect of wind: $m_0 = 59000, \gamma_{min} = 0, \gamma_{max} = 0.15, x_f = 150000$, $a_w^1 = 0.2 \times 10^{-6}, a_w^2 = 0.2$

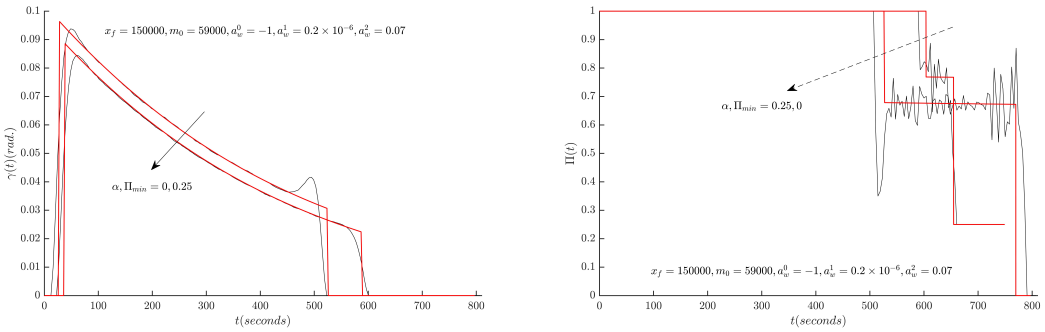

(a) (b)

Figure 13: BSB+BSB: comparison between the analytical solutions (red lines) and numerical solutions (black lines)

For $\det[M]$ to be zero, the right hand side of Eq. (86) needs to vanish. Therefore:

$$-\mathcal{L}\mathcal{A}_4 - \hat{F}_4\big(\frac{\partial \mathcal{L}}{\partial X}\big)F_{s,\gamma} = 0 \tag{87}$$

$$\mathcal{L}\mathcal{A}_4 + \hat{F}_4\big(\frac{\partial \mathcal{L}}{\partial X}\big)F_{s,\gamma} = 0 \tag{88}$$

$$-\mathcal{L}(\mathcal{A}_3 F_{s2,\gamma} - \mathcal{A}_2 F_{s3,\gamma}) - (\hat{F}_3 F_{s2,\gamma})\big(\frac{\partial \mathcal{L}}{\partial X}\big)F_{s,\gamma} = 0 \tag{89}$$

On the other hand:

$$\det[M] = \mathcal{A}_3\hat{F}_4F_{s2,\gamma} - \mathcal{A}_2\hat{F}_4F_{s3,\gamma} - \mathcal{A}_4\hat{F}_3F_{s2,\gamma} \tag{90}$$

The vector elements of $\mathcal{A}$ are:

$$\mathcal{A}_j = \Sigma_{i=1}^{4}\frac{\partial F_{sj,\gamma}}{\partial X_i}\hat{F}_i - \Sigma_{i=1}^{4}\frac{\partial \hat{F}_j}{\partial X_i}F_{si,\gamma}, \quad j = 1,2,3,4 \tag{91}$$

Eq. (87), or equivalently Eq. (88), together with $\mathcal{A}_4$, from Eq. (91), give:

$$\mathcal{L} = c(x,m)\hat{F}_4 \tag{92}$$

With Eq. (92), it is straightforward to verify that Eq. (89) corresponds to $\det[M] = 0$ and the proof is complete. □

Corollary 1. *For the minimum fuel OCP, $\mathcal{L} := -\hat{F}_4$. Therefore, from theorem 5, the singular arc for $\gamma(t)$ ($\Pi(t) = \Pi_b$) can be defined in terms of the state variables by $\det[M] = 0$ if $\lambda_x(t) = 0$. This condition corresponds to the case of unconstrained horizon, i.e., unspecified $x(t_f)$ and $w = w(h)$.*

Theorem 6. *For the objective function $\mathcal{L} := -\hat{F}_4 = -\Pi F_{s4,\Pi}$, the singular arc of $\Pi(t)$ is defined in terms of the state variables by $\det[M'] = 0$ if $\lambda_x(t) = 0$.*

Proof. On using the expressions for M' and R' (given by Eq. (62) and Eq. (63) respectively) together with $\hat{\bar{F}}_4 = 0$ ($\hat{\bar{F}} := \bar{F} + \gamma_b F_{s,\gamma}$), $\mathcal{L}_{s2,\Pi} = 0$ and $\lambda_x(t) = 0$ we have:

$$\det[M']\begin{pmatrix}\lambda_h\\ \lambda_v\\ \lambda_m\end{pmatrix} = \begin{pmatrix}\mathcal{B}_4F_{s3,\Pi} - \mathcal{B}_3F_{s4,\Pi} & -\mathcal{B}_4\hat{\bar{F}}_3 & \hat{\bar{F}}_3F_{s4,\Pi}\\ \mathcal{B}_2F_{s4,\Pi} & \mathcal{B}_4\hat{\bar{F}}_2 & -\hat{\bar{F}}_2F_{s4,\Pi}\\ -\mathcal{B}_2F_{s3,\Pi} & \mathcal{B}_2\hat{\bar{F}}_3 - \mathcal{B}_3\hat{\bar{F}}_2 & \hat{\bar{F}}_2F_{s3,\Pi}\end{pmatrix}\begin{pmatrix}-\bar{\mathcal{L}}\\ -\mathcal{L}_{s,\Pi}\\ \frac{\partial\bar{\mathcal{L}}}{\partial X}F_{s,\Pi} - \frac{\partial\mathcal{L}_{s,\Pi}}{\partial X}\hat{\bar{F}}\end{pmatrix} \tag{93}$$

On setting $\bar{\mathcal{L}} = 0$, $\mathcal{L}_{s,\Pi} = -F_{s4,\Pi}$, the right hand side of Eq. (93) becomes:

$$-\mathcal{B}_4 + \frac{\partial F_{s4,\Pi}}{\partial X}\hat{\bar{F}} = 0 \tag{94}$$

$$-\frac{\partial F_{s4,\Pi}}{\partial X}\hat{\bar{F}} + \mathcal{B}_4 = 0 \tag{95}$$

$$F_{s4,\Pi}\big(\mathcal{B}_2\hat{\bar{F}}_3 - \mathcal{B}_3\hat{\bar{F}}_2\big) + \hat{\bar{F}}_2F_{s3,\Pi}\frac{\partial F_{s4,\Pi}}{\partial X}\hat{\bar{F}} = 0 \tag{96}$$

On the other hand:

$$\det[M'] = \mathcal{B}_2\hat{\bar{F}}_3F_{s4,\Pi} - \mathcal{B}_3\hat{\bar{F}}_2F_{s4,\Pi} + \mathcal{B}_4\hat{\bar{F}}_2F_{s3,\Pi} \tag{97}$$

$$\mathcal{B}_j = \Sigma_{i=1}^{4}\frac{\partial F_{sj,\Pi}}{\partial X_i}\hat{\bar{F}}_i - \Sigma_{i=1}^{4}\frac{\partial \hat{\bar{F}}_j}{\partial X_i}F_{si,\Pi}, \quad j = 1,2,3,4 \tag{98}$$

On accounting $\mathcal{B}_4$ from Eq. (98), it is straightforward to approve that Eq. (94) and Eq. (95) are automatically satisfied and Eq. (96) is equivalent to $\det[M'] = 0$. □

Theorem 7. *In the case that $\hat{F}_4 = 0$, the singular arc for $\gamma(t)$ is defined in terms of the state variables through $\det[M] = 0$ if $\mathcal{L} = d(x)\hat{F}_1$.*

Proof. Since $\hat{F}_4 = 0$, $\frac{dm}{dt} = 0$. Therefore, the co-state dynamics, Eq. (37), Eq. (38) and Eq. (39) become:

$$\det[M] \begin{pmatrix} \lambda_x \\ \lambda_h \\ \lambda_v \end{pmatrix} = adj \begin{pmatrix} \hat{F}_1 & 0 & \hat{F}_3 \\ 0 & F_{s2,\gamma} & F_{s3,\gamma} \\ \mathcal{A}_1 & \mathcal{A}_2 & \mathcal{A}_3 \end{pmatrix} \begin{pmatrix} -\mathcal{L} \\ 0 \\ \frac{\partial \mathcal{L}}{\partial X} F_{s,\gamma} \end{pmatrix} \tag{99}$$

In order to have $\det[M] = 0$, RHS of Eq. (99) must vanish:

$$\mathcal{L}\big(\mathcal{A}_2 F_{s3,\gamma} - \mathcal{A}_3 F_{s2,\gamma}\big) - \hat{F}_3 F_{s2,\gamma} \frac{\partial \mathcal{L}}{\partial X} F_{s,\gamma} = 0 \tag{100}$$

$$-\mathcal{A}_1 \mathcal{L} - \hat{F}_1 \frac{\partial \mathcal{L}}{\partial X} F_{s,\gamma} = 0 \tag{101}$$

$$\mathcal{A}_1 \mathcal{L} + \hat{F}_1 \frac{\partial \mathcal{L}}{\partial X} F_{s,\gamma} = 0 \tag{102}$$

On the other hand:

$$\det[M] = \mathcal{A}_3 \hat{F}_1 F_{s2,\gamma} - \mathcal{A}_2 \hat{F}_1 F_{s3,\gamma} - \mathcal{A}_1 \hat{F}_3 F_{s2,\gamma} \tag{103}$$

and:

$$\mathcal{A}_1 = \Sigma_{i=1}^{3} \frac{\partial F_{s1,\gamma}}{\partial X_i} \hat{F}_i - \Sigma_{i=1}^{3} \frac{\partial \hat{F}_1}{\partial X_i} F_{si,\gamma} = -\frac{\partial \hat{F}_1}{\partial X} F_{s,\gamma} \tag{104}$$

From Eq. (104), together with Eq. (101), or equivalently Eq. (102),

$$\mathcal{L} = d(x) \hat{F}_1 \tag{105}$$

Plugging Eq. (105) into Eq. (100), gives $\det[M] = 0$. □

Corollary 2. *On setting $d(x) = -1$ in theorem 7, we have, $\mathcal{L} = -\hat{F}_1 = -(v + w)$. On the other hand, $\hat{F}_4 = 0$ is equivalent to $\Pi(t) = 0$. Therefore, it becomes lucid that this case is applicable to an un-powered descent with the maximum range, being the objective function.*

A Appendix B

In view of a parameter optimization we recast the shooting problem as:

$$\begin{aligned} &\min_{\lambda_x(t^*), \tilde{t}_k, k=1,\ldots,K \in \mathbb{N}} \mathcal{J} = \Phi(X(\tilde{t}_K), \tilde{t}_K) \\ &s.t. \\ &\frac{dX}{dt} = F(X, \lambda_x(t^*)) \\ &\phi_0(X(t_0), t_0) = 0 \\ &\phi_f(X(\tilde{t}_K), \tilde{t}_K) = 0 \end{aligned} \tag{106}$$

Since we have the expressions for the optimal controls over the extremals, the parameter optimization contains only the missing parameters, i.e., $\lambda_x(t^*)$, and the number of the extremals, $\tilde{t}_k$.

The time domain is accumulation of the time intervals:

$$\Omega = \bigcup_{k=1}^{K} \Omega_k(\tilde{t}_{k-1}, \tilde{t}_k) \tag{107}$$

The numerical integration is performed over each subdomain, Ω_k (with an equidistant mesh):

$$\Delta\tilde{t}_k = \frac{\tilde{t}_k - \tilde{t}_{k-1}}{N_k} = t_j - t_{j-1}, \quad j = 1 + \sum_{i=1}^{k-1} N_i, ..., \sum_{i=1}^{k} N_i, \quad k = 1, 2, ..., K \tag{108}$$

For a better understanding and also to simulate the presence of the state multipliers, co-states, we form the Lagrangian as:

$$\mathcal{J} = \Phi(X(\tilde{t}_K), \tilde{t}_K) + \nu_0^T \phi_0 + \nu_K^T \phi_K + \sum_{j=1}^{N} \lambda_j^T \Lambda_j, \quad N = \sum_{k=1}^{K} N_k \tag{109}$$

Λ is the state deficiency in the discrete points, t_j, verifying the presence of co-states, λ:

$$\Lambda_j = \tilde{X}(t_j) - X(t_j) \tag{110}$$

$\tilde{X}(t_j)$ is the expanded field about $X(t_{j-1})$. In order to facilitate understanding the optimization process, we take a basic Euler expansion:

$$\tilde{X}(t_j) = X(t_{j-1}) + F\big(X(t_{j-1}), \lambda_x(t^*)\big)(t_j - t_{j-1}) \tag{111}$$

Therefore:

$$\begin{aligned} &\mathcal{J} = \Phi(X(\tilde{t}_K), \tilde{t}_K) + \nu_0^T \phi_0 + \nu_K^T \phi_K + \\ &\sum_{k=1}^{K} \sum_{j=1+\sum_{i=1}^{k-1} N_i}^{\sum_{i=1}^{k} N_i} \lambda_j^T \Big(X(t_{j-1}) - X(t_j) + F\big(X(t_{j-1}), \lambda_x(t^*)\big)\Delta\tilde{t}_k \Big) \end{aligned} \tag{112}$$

The KKT condition for $\tilde{t}_k$ instates:

$$\frac{\partial \mathcal{J}}{\partial \tilde{t}_k} = 0, \quad k = 1, .., K \tag{113}$$

For the interior points, i.e., $k = 1, .., K-1$, the KKT condition involves the adjacent extremals, $\Delta\tilde{t}_k$ and $\Delta\tilde{t}_{k+1}$. Therefore:

$$\frac{\partial \mathcal{J}}{\partial \tilde{t}_k} = \frac{1}{N_k} \sum_{j=1+\sum_{i=1}^{k-1} N_i}^{\sum_{i=1}^{k} N_i} \lambda_j^T F\big(X(t_{j-1}), \lambda_x(t^*)\big) - \frac{1}{N_{k+1}} \sum_{j=1+\sum_{i=1}^{k} N_i}^{\sum_{i=1}^{k+1} N_i} \lambda_j^T F\big(X(t_{j-1}), \lambda_x(t^*)\big) = 0 \tag{114}$$

On the hand, the discrete Hamiltonian for this system is $\mathcal{H}_j = \lambda_j^T F\big(X(t_j), \lambda_x(t^*)\big)$. Therefore, on defining a deficient Hamiltonian, $\tilde{\mathcal{H}}_j = \lambda_j^T F\big(X(t_{j-1}), \lambda_x(t^*)\big)$, one arrives at:

$$\bar{\tilde{H}}_k = \bar{\tilde{H}}_{k+1} \tag{115}$$

With:

$$\bar{\tilde{H}}_k = \frac{1}{N_k} \sum_{j=1+\sum_{i=1}^{k-1} N_i}^{\sum_{i=1}^{k} N_i} \lambda_j^T F\big(X(t_{j-1}), \lambda_x(t^*)\big), \quad k = 1, 2, ..., K-1 \tag{116}$$

For the boundary point, $k = K$:

$$\frac{\partial \mathcal{J}}{\partial \tilde{t}_K} = \frac{\partial \Phi}{\partial \tilde{t}_K} + \nu_K^T \frac{\partial \phi_K}{\partial \tilde{t}_K} + \frac{1}{N_K} \sum_{j=1+\sum_{i=1}^{K-1} N_i}^{\sum_{i=1}^{K} N_i} \lambda_j^T F\big(X(t_{j-1}), \lambda_x(t^*)\big) = \frac{\partial \Phi}{\partial \tilde{t}_K} + \nu_K^T \frac{\partial \phi_K}{\partial \tilde{t}_K} + \bar{\tilde{\mathcal{H}}}_K = 0 \tag{117}$$

In short, Eq. (115) and Eq. (116) correspond to the uniformity of Hamiltonian and the transversality condition for an autonomous system in Mayer form.

In the case that $N_k = 1, k = 1, 2, ..., K = N$, ... gives:

$$\tilde{\mathcal{H}}_j = \tilde{\mathcal{H}}_{j+1}, \quad j = 1, 2, ..., N \tag{118}$$

Together with the assumption, $N \to \infty$:

$$d(\tilde{\mathcal{H}}) = 0 \tag{119}$$

Therefore, it becomes perspicuous that the junction points correspond to the uniformity of Hamiltonian over the adjacent extremals.

It turns out that a very sparse parameter optimization over the parameters, $\tilde{t}_k, \lambda_x(t^*)$ is remarkably accurate compared to a shooting translation and hence, it is a logical alternative (see table 6). The data in table 6 are from a simulation with $\mathcal{L} = 1$ and $No\ Wind$ condition. The optimal $\gamma(t)$ and $\Pi(t)$ were confirmed BSB and B respectively. As for the shooting and parameter optimization, we used $fsolve$ and $fmincon$ from MATLAB respectively.

Table 6: Shooting (s.) vs. Parameter Optimization (p.o.) for a Minimum Time Problem: No Wind, m_0=79000, $x_{tf} = 180000$, BSB (parameters: t_1, t_2, $t_3 := t_f$, $\lambda_x(t_1)$)

Quantity	Test Case 1	Test Case 2	Test Case 3	Test Case 4
N_1	100	300	500	1000
N_2	500	500	500	1000
N_3	500	500	500	1000
$t_1(s.)$	79.1012	78.1347	77.9744	77.7547
$t_1(p.o.)$	79.0602	78.1651	77.9946	77.7574
$t_2(s.)$	819.0109	821.0051	821.4188	821.8351
$t_2(p.o.)$	818.9088	820.9962	821.4257	821.8334
$t_f(s.)$	840.5155	842.2944	842.6612	843.0167
$t_f(p.o.)$	840.5131	842.2944	842.6612	843.0167
$\lambda_x(t_1)(s.)$	-0.001533	-0.001246	-0.001191	-0.001168
$\lambda_x(t_1)(p.o.)$	-0.001656	-0.001268	-0.001180	-0.001181

References

[1] Abolfazl Simorgh, Manuel Soler, Daniel González-Arribas, Sigrun Matthes, Volker Grewe, Simone Dietmüller, Sabine Baumann, Hiroshi Yamashita, Feijia Yin, Federica Castino, Florian Linke, Benjamin Lührs, and Maximilian Mendiguchia Meuser. A comprehensive survey on climate optimal aircraft trajectory planning. *Aerospace*, 9(3), 2022.

[2] I. Michael Ross. A historical introduction to the convector mapping principle, 2005. The article of record as published may be located at http://arc.aiaa.org.

[3] M.I. Ross and F. Fahroo. Discrete verification of necessary conditions for switched nonlinear optimal control systems. In *Proceedings of the 2004 American Control Conference*, volume 2, pages 1610–1615 vol.2, 2004.

[4] Mark D. Ardema. Solution of the minimum time-to-climb problem by matched asymptotic expansions. *AIAA Journal*, 14(7):843–850, 1976.

[5] Olivier Cots, Joseph Gergaud, and Damien Goubinat. Time-optimal aircraft trajectories in climbing phase and singular perturbations. *IFAC-PapersOnLine*, 50(1):1625–1630, 2017. 20th IFAC World Congress.

[6] Nhan Nguyen. Singular arc time-optimal climb trajectory of aircraft in a two-dimensional wind field. *AIAA Guidance, Navigation, and Control Conference and Exhibit*, 2006.

[7] Antonio Franco and Damián Rivas. Optimization of multiphase aircraft trajectories using hybrid optimal control. *Journal of Guidance, Control, and Dynamics*, 38(3):452–467, 2015.

[8] Sang Gyun Park and John-Paul Clarke. Vertical trajectory optimization to minimize environmental impact in the presence of wind. *Journal of Aircraft*, 53(3):725–737, 2016.

[9] Douglas M. Pargett and Mark D. Ardema. Flight path optimization at constant altitude. *Journal of Guidance, Control, and Dynamics*, 30(4):1197–1201, 2007.

[10] J. D. Mancill. Identically non-regular problems in the calculus of variations. *Mathematica Y Fisica Teorica (Univ. Nacional del Tucuman, Republica Argentina)*, 7(2):131–139, 1950.

[11] A. Miele. Extremiziation of linear integrals by green's theorem," optimization techniques. *Academic Press, New York*, pages 69–99, 1962.

[12] Antonio Franco, Damián Rivas, and Alfonso Valenzuela. Minimum-fuel cruise at constant altitude with fixed arrival time. *Journal of Guidance, Control, and Dynamics*, 33(1):280–285, 2010.

[13] Damián Rivas and Alfonso Valenzuela. Compressibility effects on maximum range cruise at constant altitude. *Journal of Guidance, Control, and Dynamics*, 32(5):1654–1658, 2009.

[14] Olivier Cots, Joseph Gergaud, and Damien Goubinat. Direct and indirect methods in optimal control with state constraints and the climbing trajectory of an aircraft. *Optimal Control Applications and Methods*, 39, 11 2017.

[15] Antonio Franco and Damián Rivas. Analysis of optimal aircraft cruise with fixed arrival time including wind effects. *Aerospace Science and Technology*, 32(1):212–222, 2014.

[16] Antonio Franco, Damián Rivas, and Alfonso Valenzuela. Optimization of unpowered descents of commercial aircraft in altitude-dependent winds. *Journal of Aircraft*, 49(5):1460–1470, 2012.

[17] Helmut Maurer, Tanya Tarnopolskaya, and Neale Fulton. Optimal bang-bang and singular controls in collision avoidance for participants with unequal linear speeds. In *2012 IEEE 51st IEEE Conference on Decision and Control (CDC)*, pages 7697–7702, 2012.

[18] Helmut Maurer, Tanya Tarnopolskaya, and Neale Fulton. Computation of bang-bang and singular controls in collision avoidance. *Journal of Industrial and Management Optimization*, 10(2):443–460, 2014.

[19] Clara Rojas Rodríguez and Juan Belmonte-Beitia. Optimizing the delivery of combination therapy for tumors: A mathematical model. *International Journal of Biomathematics*, 10(03):1750039, 2017.

[20] Alberto d'Onofrio, Urszula Ledzewicz, Helmut Maurer, and Heinz Schättler. On optimal delivery of combination therapy for tumors. *Mathematical Biosciences*, 222(1):13–26, 2009.

[21] D. Subbaram Naidu and Anthony J. Calise. Singular perturbations and time scales in guidance and control of aerospace systems: A survey. *Journal of Guidance, Control, and Dynamics*, 24(6):1057–1078, 2001.

[22] A. Miele, T. Wang, and W. W. Melvin. Optimization and acceleration guidance of flight trajectories in a windshear. *Journal of Guidance, Control, and Dynamics*, 10(4):368–377, 1987.

[23] Michael R. Jackson, Yiyuan J. Zhao, and Rhonda A. Slattery. Sensitivity of trajectory prediction in air traffic management. *Journal of Guidance, Control, and Dynamics*, 22(2):219–228, 1999.

[24] Arthur J. Krener. The high order maximal principle and its application to singular extremals. *SIAM Journal on Control and Optimization*, 15(2):256–293, 1977.

[25] Richard F. Hartl, Suresh P. Sethi, and Raymond G. Vickson. A survey of the maximum principles for optimal control problems with state constraints. *SIAM Review*, 37(2):181–218, 1995.

[26] J. P. McDanell and W. F. Powers. Necessary conditions joining optimal singular and nonsingular subarcs. *SIAM Journal on Control*, 9(2):161–173, 1971.

[27] H. Maurer. On optimal control problems with bounded state variables and control appearing linearly. *SIAM Journal on Control and Optimization*, 15(3):345–362, 1977.

[28] D. Poles. Base of aircraft data (bada) aircraft performance modelling report. *EEC Technical/Scientific Report, Eurocontrol*, 2009.

[29] Anil V. Rao. A survey of numerical methods for optimal control. *Advances in the Astronautical Sciences*, 135(1), 2010.